

Decadal Trends in observed surface solar radiation and their causes in Brazil in the first two decades of the 21st century.

L. F. Correa^{1,2}, D. Folini¹, B. Chtirkova¹, and M. Wild¹

¹Institute for Atmospheric and Climate Sciences, ETH Zurich, Zurich, Switzerland.

²Department of Geography, LMU Munich, Munich, Germany.

Correspondence to: Lucas Ferreira Correa (lucas.ferreira@env.ethz.ch)

Abstract. Numerous studies have investigated the long term variability of surface solar radiation (SSR) around the world. However, the large disparity in the availability of observational data between developed and least developed/developing countries leads to an underrepresentation of studies on SSR changes in the latter. This is especially true for South America, where few observational studies have investigated the SSR ~~decadal~~ trends, and usually only at a local or regional scale. In this study we use data from 34 stations distributed throughout all the regions of Brazil to present the ~~decadal~~ SSR ~~decadal~~ trends in the first two decades of the 21st century and investigate their associated causes. The stations were grouped into 8 composites according to their proximity. Our results show that in the North and Northeast Brazil a strong dimming occurred, with significant contributions from increasing atmospheric absorption, most likely due to anthropogenic emissions, and increasing cloud cover. In the Southeast and Midwest regions of Brazil near-zero trends resulted from competing effects of clear-sky processes (attenuation of solar radiation under cloudless conditions) and strong negative trends in cloud cover. In the South part of the Amazon and in Southern Brazil a statistically insignificant brightening was observed, with significant contribution from decreasing biomass burning emissions in the former and competing minor contributions in the latter. These results can contribute to deepen the knowledge and understanding of SSR ~~long-term~~~~decadal~~ trends and their causes in South America, reducing the underrepresentation of this continent when compared to regions like Europe.

1. Introduction

Decadal trends in surface solar radiation (SSR) have been the ~~object~~subject of study since pioneering studies in late 1980s and early 1990s made efforts to try to understand the long-term variation of ~~presented evidence that SSR is not constant over time, but rather undergoes decadal trends~~ (Ohmura and Lang, 1989; Russak, 1990; Dutton et al., 1991; Stanhill and Moreshet, 1992). Several studies have followed presenting the trends and discussing their causes and potential consequences in several parts of the world (Wild, 2009), such as in Europe (e.g. Manara et al., 2016; Norris and Wild, 2007; Power, 2003), North America (e.g. Liepert 2002), China (e.g. Feng and Wang, 2019; Wang et al., 2015), Japan (e.g. Kudo et al., 2012) and New Zealand (Liley, 2009). Global dimming (negative

34 trends in SSR) and brightening (positive trends in SSR) have been associated, in most of the cases, with
35 changes in cloud cover (e.g. Stjern et al., 2008; Augustine and Capotondi, 2022) and changes in aerosol
36 loadings (e.g. Wild et al., 2021, Kambezidis et al., 2012), with the dominant aspect depending on
37 regional atmospheric and emission features. However, many regions of the world are still
38 underrepresented by such studies, mostly because of the lack of observational high quality data in most
39 of developing and least developed countries in contrast to regions like Europe, North America or
40 Eastern Asia. South America is an important region to be mentioned in this context.

41 The lack of long-term SSR data in South America, reported by different authors (Ohmura,
42 2009; Gilgen et al., 2009), is the main cause for the absence of a long literature in the region. Still, a
43 few studies tried to assess SSR variability in South America. Ohmura (2009) presented and discussed
44 SSR decadal trends based on a few stations in Venezuela *at the end of the 20th century*. Schwartz (2005)
45 used astronomical extinction measurements to estimate clear-sky SSR trends at one astronomical
46 observatory in Chile *during two decades (1978-1997)*. Yuan et al. (2021) and Jiao et al. (2023) used
47 machine learning methods to spatially interpolate SSR ground observations *and reanalysis data* and
48 used this approach to assess SSR decadal variability over the whole globe, including South America,
49 *covering the second half of the 20th century and the first two decades of the 21st century*. Da Silva et
50 al. (2010), de Jong et al. (2019) and de Lima et al. (2019) all assessed SSR variability in Brazil with a
51 focus on the potential for photovoltaic energy production. Zuluaga et al. (2021) and Raichijk (2012)
52 used sunshine duration to assess the SSR variability in Brazil *for the last 2 to 4 decades of the 20th*
53 *century and the beginning of the 21st century*. A similarity between most of these studies is the fact that
54 they had to rely on reanalysis, modeling data and indirect estimators of SSR (like sunshine duration),
55 with the only of the abovementioned studies that used ground observations being limited to a small
56 region in Venezuela. This leaves regions such as the densely populated southeastern Brazil or the highly
57 climate-relevant Amazon region without any direct assessment of the regional SSR long term
58 variability. Yamasoe et al. (2021) presented and discussed a SSR time series of fifty-six years *(1961-*
59 *2016)* measured in the city of Sao Paulo, and that is, to our knowledge, the longest and most detailed
60 analysis of directly observed SSR in South America. *The studies referenced here apply different*
61 *methods, to different regions, in different periods, so it is hard to directly compare them. But, in general*
62 *terms, studies based on sunshine duration tend to indicate a brightening in Brazil after 1980s, while*
63 *studies using machine learning techniques and regional observational studies show a spatial*
64 *heterogeneity in the SSR trends in Brazil in the last few decades*. All these studies provide different
65 pieces of information about SSR variability in this part of the world, however, none of them provide a
66 large scale assessment of the long term SSR decadal trends using ground observations of SSR, as done
67 for regions like Europe (e.g. Chiacchio and Wild, 2010; Pfeifroth et al., 2018), China (e.g. Yang et al.,
68 2018) or the United States (e.g. Long et al., 2009).

69 To try to tackle this gap in literature, we made use of the availability of SSR data from
70 automated meteorological stations from the Instituto Brasileiro de Meteorologia (INMET) from 2001

71 onwards to provide a large scale assessment of SSR decadal trends and underlying causes at the
72 beginning of the 21st century in the Brazilian territory, which covers approximately half of the South
73 American continent. The direct assessment of SSR long-term variability (using observed SSR) over
74 such a large area in South America represents a novel contribution from this work. The objective of this
75 study is to present the in-situ observed SSR decadal trends around Brazil in the first two decades of the
76 21st century and discuss their underlying causes. This is done at the regional level, rather than locally,
77 by selecting stations in strategic locations around the Brazilian territory and grouping them into station
78 composites. With this study we intend to help to reduce the under representativity of Global Dimming
79 and Brightening (GDB) studies in South America.

80 2. Data and methods

81 2.1 In situ SSR and cloud cover measurements

82 Surface solar radiation data for 32 of the 34 stations (see table 3, in annex) is collected and
83 controlled by the Instituto Brasileiro Nacional de Meteorologia (INMET) and was retrieved from the
84 BDMEP portal (available at: <https://bdmep.inmet.gov.br/> (last access 27 Oct 2023)). The stations were
85 chosen based on data availability in the regions of each composite used in this study (see section 2.4).
86 The data was retrieved at hourly time resolution. All data was tested at the hourly time scale for
87 consistency using the physical and extremely rare limits established by Long and Dutton (2002). None
88 of the INMET stations used in this study were reported to have major discontinuities in the records.
89 Nevertheless, we still applied the penalized maximal F test by Wang (2008) to verify the time series for
90 inhomogeneities. No homogeneity problems were identified in the stations used in this study. The
91 hourly values were further converted into daily means by simply averaging the 24 hourly values in a
92 day. If one hourly value was missing (due to either lack of data or removal during quality test) the one
93 hourly value was filled linearly using the previous and next hours and the daily value was the average
94 of 24 hourly values (23 observed and 1 filled linearly). If more than one hourly value was missing, the
95 daily value was not calculated. Daily values were further converted into monthly values by simply
96 averaging the daily means within the same month. Monthly values were only calculated when at least
97 70% of the days in a month were available. Further conversion from monthly to annual values again
98 occurred by simply averaging the 12 months. If one, ~~or~~ two or three monthly values went missing, the
99 long term mean (mean for the whole period with available data) for that month would be used instead,
100 and the annual mean was still calculated. If more than ~~three~~ monthly values were missing, then the
101 annual value was not calculated. The averaging procedure from daily to monthly, and from monthly to
102 annual values reproduces similar methodologies used in previous studies (e.g. Stjern et al., 2008;
103 Manara et al., 2016).

104 The BSRN (Baseline Surface Radiation Network, Ohmura et al., 1998; Driemel et al., 2018)
105 station at Florianopolis was also used in this study. Its data was provided at 15-minute intervals. Data

106 from the station operated by the Instituto de Astronomia, Geofisica e Ciencias Atmosfericas of the
107 Universidade de São Paulo (IAG/USP), located in the city of Sao Paulo was also used. Data from this
108 station was provided as daily means. Both time series were also checked for consistency with the same
109 procedure applied to the INMET stations, at the hourly time scale for the BSRN station and at the daily
110 time scale for the IAG/USP station. Metadata for both stations did not report any discontinuities, and
111 the tests performed using the penalized maximal F test by Wang (2008) also did not indicate any
112 inhomogeneity in the time series. -The SSR long term variability at the Sao Paulo station was previously
113 carefully analyzed by Yamasoe et al. (2021). This station also has the longest time coverage among all
114 of the stations used in this study: all the other stations only have data after 2000, while this stations has
115 available data from decades earlier. But we limited the analysis to the period with coverage of the other
116 stations because we intend to investigate the SSR variability at the regional level (composites) rather
117 than at the local level (individual station). The procedure to convert from sub-daily to daily averages,
118 from daily to monthly and from monthly to annual values at these two stations was the same as the
119 procedure used for the INMET stations.

120 Cloud cover data was also retrieved through the BDMEP portal from the INMET. The stations
121 were the same as used for the INMET SSR measurements with the addition of data from Florianopolis.
122 In Florianopolis, where the SSR data is originally from BSRN, the location of the SSR and the cloud
123 measurements differ by a few kilometers. Cloud cover data is collected from visual inspections at 00,
124 12 and 18 UTC and is provided in units of tenths (1/10) of cloud cover.. The daily cloud cover values
125 used in this study are a result of the average from the 12 and 18 UTC observations. This is equivalent
126 to 9 and 15 local time at most of the stations used in this study (8 and 14 for the westernmost stations).
127 At the Sao Paulo station, the diurnal cloud cover values are a result of hourly observations between 7
128 and 18 local time. Cloud cover data was converted into monthly and then annual values using the same
129 procedure as used for the SSR data. The cloud cover data is also used to calculate the Cloud Cover
130 Radiative Effect (CCRE), following the procedure described by Norris and Wild (2007). This variable
131 gives an estimation of the change in SSR produced by changes in cloud cover.

132 The SSR data described in this section is used to estimate the SSR trends presented in table 1,
133 and to calculate the fractional atmospheric column absorption (see section 2.4), which also has the
134 trends presented in table 1. The cloud cover data described in this section was used to estimate cloud
135 cover trends presented in table 1 and to apply one of the two methods for clear-sky identification used
136 in this study (see section 2.3).

137 2.2 Satellite and reanalysis data

138 To investigate Aerosol Optical Depth (AOD) variability, we used data from the CAMS
139 (Copernicus Atmosphere Monitoring System) reanalysis (Inness et al., 2019), provided by ECMWF.
140 This product has monthly time steps and spatial resolution of approximately 80 km, with temporal
141 coverage starting from 2003. Gueymard and Yang (2020) validated CAMS data using AERONET

142 stations from around the world, including South America and found that the reanalysis performs well
143 in comparison to in-situ aerosol observations, therefore being well suited for regional and global studies.
144 To assess the Aerosol Absorption Optical Depth (AAOD) at 500 nm we used data from the OMAERUV
145 aerosol algorithm from the Ozone Monitoring Instrument (OMI, Torres et al., 2007). The product is
146 provided at daily time resolution and 1-degree resolution, and is available from 2004 onwards. Due to
147 the frequent occurrence of missing daily values in the AAOD data from OMI (due to different aspects,
148 such as cloudy scenes), conversion from daily to monthly values was done only when at least two days
149 in a month were available. From monthly to annual values the conversion was only performed when at
150 least 11 of the 12 months had available data (missing month would be filled with long term mean, that
151 is, the mean for the whole period with data availability). We should also highlight that aerosol
152 absorption is a variable highly dependent on the spectral region, thus the absorption at 500 nm could
153 not be representative for the whole spectrum.

154 We also used shortwave radiative fluxes measured at the Top of the Atmosphere (TOA) by the
155 CERES (Cloud and Earth's Radiant Energy System, Doelling et al., 2013) instruments on board of the
156 satellites Terra and Aqua. The CERES-~~EBAF~~SSF product (LeebDoelling et al., 2016~~8~~), used in this
157 study, provided TOA shortwave fluxes at monthly time intervals and 1-degree spatial resolution, from
158 2000 onwards. The same product also provided incoming shortwave radiative fluxes at the TOA, which
159 was also used in this study. The data from CERES was used to estimate fractional atmospheric column
160 absorption (see section 2.4).

161 Anthropogenic emissions were assessed using EDGAR (Emissions Database for Global
162 Atmospheric Research, Crippa et al., 2018). The data provides anthropogenic emission estimates at 0.1
163 degree spatial resolution and does not consider large scale biomass burning, land use change and
164 forestry (Crippa et al., 2018). This dataset was used, even though it does not include biomass burning,
165 because it provides information about aerosol emissions from all other sources, which are also relevant,
166 such as urban and industrial emissions. For this study we acquired the data in annual values and in units
167 of $\text{kg m}^{-1} \text{s}^{-1}$. The unit was further converted to $\text{kg grid}^{-1} \text{year}^{-1}$ (kg emitted for each 0.1 degree grid per
168 year). Finally, total column water vapour was obtained from the ERA5 reanalysis (Hersbach et al.,
169 2020), which provides data with a 0.25 degree spatial resolution and monthly time resolution. Cloud
170 cover from ERA5 was also used as supporting information in addition to the previously mentioned
171 SYNOP cloud cover, measured in-situ.

172 The AOD, AAOD, water vapor and anthropogenic emissions data described in this section were
173 used to identify the spatial distribution of the trends for these variables. The TOA incoming and
174 outgoing irradiance data described in this section was used to estimate fractional atmospheric column
175 absorption (see section 2.4). For all gridded data described in this section, the stations were sampled by
176 taking the grid box containing the station coordinates.

177

178 **2.3 Clear-sky SSR**

179 Time series of clear-sky SSR were derived using two different methods. At all stations we used
180 (1) the clear-sky method proposed by Correa et al. (2022), and at the stations with Synop cloud cover
181 data we also (2) derived clear-sky using cloud cover information. We applied both methods on the daily
182 time series. For the first method, we calculate station specific daily transmittance thresholds for every
183 month of the year. Days with transmittance lower than this threshold for the specific station in the
184 respective month are flagged as cloudy and removed. Days with transmittance above the thresholds are
185 flagged as clear-sky. As this method relies on the reduction of atmospheric transmittance under cloudy
186 conditions, its main weakness is associated with extreme aerosol events that could suddenly strongly
187 reduce transmittance. Thus this method is not well suited for the analysis of high frequency (interannual)
188 variability, but it has been shown adequate for assessment of long term trends (Correa et al., 2022).

189 For the second method, we simply used in-situ observations of cloud cover to identify cloudy
190 scenes. We set the threshold of cloud cover to two tenths (20%), where any day with cloud cover above
191 that was flagged as cloudy and removed. The choice of the cloud cover threshold represents a trade-off,
192 where low thresholds (say, 0%) would completely avoid any cloud signal but would also remove days
193 with low cloud occurrence, where the effects of cloud-free processes still dominate, and leave the time
194 series with very few valid values. For this reason, we allowed a higher threshold, assuming that on days
195 with such low cloud cover (0-20%) the cloud-free processes still dominate the signal of the SSR
196 variability.

197 In both methods, the removal of cloudy days results in clear-sky SSR time series with many
198 gaps. Thus, special care should be taken when converting from daily to monthly values and from
199 monthly to annual values. Monthly values were only calculated when at least two daily values were
200 available for the respective month. But before taking their average, each available daily value is
201 normalized to the 15th day of the month by multiplying the daily irradiance with a normalization factor.
202 This normalization factor is a result of the ratio between the TOA daily irradiance at the 15th day of the
203 month and at the day flagged as clear-sky. This is done to correct for the solar geometry at different
204 times of the month. From monthly to annual values the procedure is the same as done for all-sky SSR:
205 the calculation is done when at least 10 months are available, with missing values being replaced by
206 long term means. When less than 10 months are available, the annual means are not calculated.

207

208 **2.4 Fractional atmospheric column absorption**

209 The daily fractional atmospheric column absorption (F_{abs}) was calculated for every station by
210 combining SSR measured at the surface, surface albedo from ERA5 at the 0.25x0.25 degree spatial
211 resolution and incoming and outgoing shortwave radiation at TOA from CERES-SSF 1deg from the
212 Terra satellite (1x1 degree spatial resolution) and daily time resolution. For the gridded data the pixel

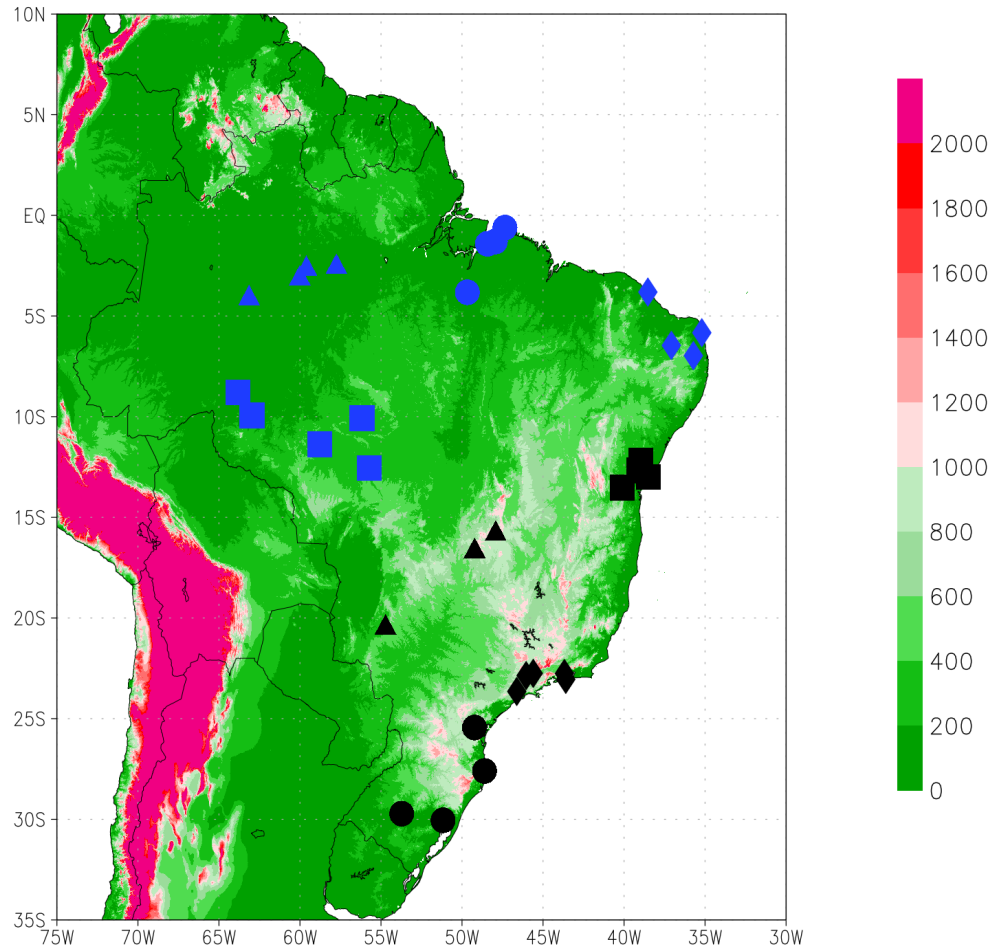
containing the station coordinates was used.- These variables were combined in equation 1 to calculate F_{abs} .

$$F_{abs} = 1 - (SW_{upTOA}/SW_{downTOA}) - ((1-\text{albedo}_{SFC})*(SW_{downSFC}/SW_{downTOA})) \quad (1)$$

SW_{upTOA} is the outgoing shortwave radiation at TOA, $SW_{downTOA}$ is the incoming shortwave radiation at TOA, albedo_{SFC} is the surface albedo and $SW_{downSFC}$ is the SSR. Thus, the term $(SW_{upTOA}/SW_{downTOA})$ represents the fraction (0-1) of the incoming shortwave radiation at the TOA which is reflected back to space, and the term $((1-\text{albedo}_{SFC})*(SW_{downSFC}/SW_{downTOA}))$ represents the fraction (0-1) of the incoming shortwave radiation at the TOA which is absorbed at the surface. Then, F_{abs} represent the fraction of the incoming shortwave radiation at TOA which is absorbed within the atmosphere column. F_{abs} values can range between 0 and 1, where 0 would represent no atmospheric absorption and 1 would represent a black body absorption by the atmosphere.

2.5 Selection of station composites

The stations used in this study were divided into eight composites based on geographical proximity, demographics and atmospheric features found in Brazil. That is, the composites were organized with the intent of covering different climate characteristics around the country and, when possible in most cases, included data from big cities (> 1 million inhabitants). The use of data from big cities for cities better spatial reference facilitates the construction of the composite time series, since the stations with longest time series and less missing data were found near big centers. The composites are: [1] Manaus region, [2] Belem region, [3] Fortaleza region, [4] Salvador region, [5] South Amazon, [6] Midwest Brazil, [7] Southeast Brazil and [8] South Brazil. The location of all stations are shown in Figure 1, and colors and markers denote the different composites. Each composite is composed of three to five stations. Based on literature review, Reboita et al. (2010) divided the precipitation regimes in South America in 8 regions, out of which five regions occurred in the Brazilian territory. Ferreira and Reboita (2022) revisited the topic and applied a non-hierarchical clustering technique to classify the precipitation regimes in South America. The authors also found 8 different precipitation regimes in the continent and only minor spatial differences to the previous study, with five of the regimes being present in the Brazilian territory. All of them were at least partly represented by the composites.



241 **Figure 1: Map of Surface Solar Radiation stations and composites used in this study and topography of**
 242 **South America (in meters above sea level). Colors and shapes represent the different composites: Blue**
 243 **triangles**Black = Manaus region; PurpleBlue circles = Belem region; Blue diamondsGreen = Fortaleza
 244 **region; RedBlack squares = Salvador region; Light BlueBlue squares = South Amazon; YellowBlack**
 245 **triangles = Midwest Brazil; Dark blueBlack diamonds = Southeast Brazil; WhiteBlack circles = South**
 246 **Brazil.**
 247

248 In the north of Brazil two composites were centered around the two biggest cities in the
 249 Brazilian Amazon, (1) Manaus and (2) Belem. Precipitation and cloudiness in both regions is strongly
 250 tied to local to mesoscale phenomena, like local convection, sea breeze circulation and squall lines. At
 251 the large scale, with the Intertropical Convergence Zone (ITCZ) being the most important large
 252 scale also has a significant influence on the precipitation in the regions phenomena, playing a major role
 253 for the seasonality of precipitation (Fisch et al., 1998). Feedbacks with the Amazon rainforest are also
 254 important, especially the recycling of precipitation. But regarding biomass burning in the Amazon, the
 255 most important area is located in the southern part of the Amazon (Artaxo et al., 2006), south of both
 256 Belem and Manaus locations. The occurrence of the South American Low Level Jet (Vera et al., 2006),
 257 important for moisture and aerosol transport from the Amazon to Southeastern Brazil, leaves the

258 locations of Belem and Manaus ~~out of the area with the strongest influence of biomass burning aerosols~~
259 ~~from the Amazon~~ with lower influence of biomass burning aerosols than the southern fraction of the
260 Amazon. Still, the influence of aerosols from the forests (either biogenic or biomass burning related)
261 should not be neglected (Rosario et al., 2019), and most importantly, the importance of anthropogenic
262 emissions from such big population centers should be taken into account.

263 In the northeast of Brazil, the composites of (3) Fortaleza and (4) Salvador share similar general
264 characteristics regarding precipitation and cloudiness regimes. The stations in these composites are also
265 centered around big population centers (Fortaleza and Salvador), where anthropogenic emissions
266 should be taken into account. The biggest difference to the composites around Manaus and Belem, is
267 that these two composites are not located in the Amazon region. But they are located in the same
268 precipitation regime division proposed by by Ferreira and Reboita (2022), with two stations of the
269 Fortaleza composite being located in a different subdivision.

270 The composite (5), South Amazon, was chosen to cover the region under the strongest influence
271 of biomass burning aerosols from the Amazon (Artaxo et al., 2006). The stations in this composite are
272 located in a different subdivision by Ferreira and Reboita (2022), where large scale phenomena (such
273 as the Bolivian high, the South Atlantic Convergence Zone and cold fronts) play an important role for
274 the cloud formation. This composite is not centered around a big city, and the most populated city in
275 the area is Porto Velho, with a population of approximately 500'000 people (IBGE, 2022). A few
276 degrees south of the South Amazon composite, are the stations of the (6) Middle West Brazil composite.
277 They are located approximately halfway between the South Amazon composite and the densely
278 populated Southeast Brazil. It is a dry region mostly influenced by large scale phenomena, compared
279 to the north and northeast regions of Brazil. The biggest city in the composite is Brasilia.

280 The Southeast is the most densely populated area in Brazil, where big centers like Sao Paulo
281 and Rio de Janeiro are located. Like the Middle West and South Amazon composites, cloud formation
282 in this region is mostly associated with large scale phenomena, ~~with significant influence from local~~
283 ~~convection and sea breeze being limited mostly to summer months~~ (Reboita et al., 2010; Ferreira and
284 Reboita, 2022). The (7) Southeast Brazil composite covers this area. The transport of humidity and
285 aerosols from the south Amazon are both relevant aspects to consider. But regarding aerosols, ~~urban-~~
286 ~~industrialanthropogenic~~ emissions from the large population centers should be more relevant. The last
287 station composite covers the Southernmost part of the country. The (8) South Brazil composite is
288 entirely located in subtropical latitudes, and covers its own precipitation regime subdivision from
289 Ferreira and Reboita (2022). Large scale phenomena like frontal ~~systemss~~ and ~~extra-sub~~tropical
290 cyclones play a major role for cloud formation and moisture transport from the ocean. It is also a densely
291 populated region, with big cities like Porto Alegre, Curitiba and Florianopolis, thus,
292 ~~anthropogenic~~ ~~urban-industrial~~ aerosol emissions should be taken into account.

293 The whole discussion in this study revolves around these eight composites. Each variable was
294 fully processed and converted to annual values at the station level, and only after that, they were grouped

295 with the other stations in the respective composite. The list of stations in each composite can be found
296 in Table 32 (in appendix).

297 **2.6 Trend calculations**

298 The trend analysis was based on annual anomalies of SSR. To calculate the annual anomalies,
299 the absolute SSR annual values were subtracted from the average SSR value for the whole period of
300 data availability for the respective composite (see table 1). This did not affect the trends, but facilitated
301 the visualization and comparison between time series, since the anomalies are centered around a
302 common value (zero). Decadal trends of SSR and most other variables presented in this study were
303 calculated using a Linear Least Squares (LLS) regression, with the confidence intervals (at the 95%
304 confidence level) being calculated using equation 4 from Nishizawa and Yoden (2005). Cloud cover
305 time series, in most cases, did not have the residuals normally distributed, thus, to account for that, we
306 calculated their trends using the Sen's slope (Sen, 1968) and Mann-Kendall test (Mann, 1945; Kendall,
307 1975). Trends of ground observations were calculated for the whole time availability of the composites,
308 however, as the time availability varies from one composite to the other, the periods used for trend
309 calculations vary by a few years. SSR trends are displayed in units of W/m^2 per decade. The period
310 considered in each composite is displayed in Table 1.

311

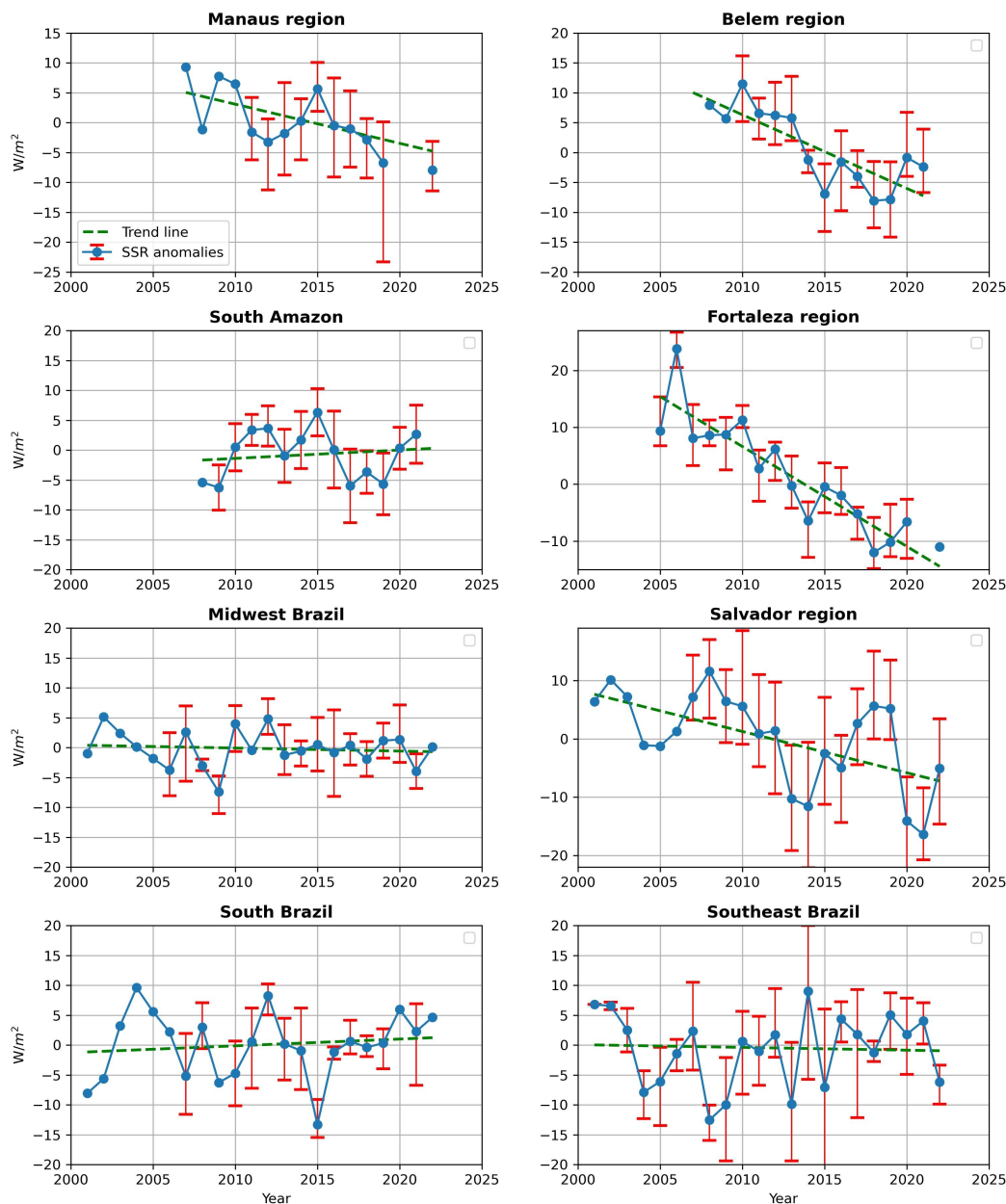
312 **3. Results**

313 **3.1 All-sky and clear-sky SSR trends**

314 Figure 2 shows the all-sky SSR anomalies time series of the 8 composites analyzed in this
315 study. All trends calculated in this study are shown in Table 1.

316

317



318

319

320

321

322

323

324

325

Figure 2: Time series of all-sky Surface Solar Radiation annual anomalies from the eight composites used in this study. Each composite is composed of three to five stations. In each composite, anomalies are in reference with respect to the mean composites of the entire period (shown in table 1). The error bars indicate the maximum and minimum value for the individual stations in the respective year and composite. Trends are indicated by dashed lines.

Composites	Period	All-sky	Clear-sky (Correa et al., 2022)	Clear-sky (Synop)*	Synop Cloud cover	All-sky atm abs	Clear-sky atm abs	CCRE
Manaus region	2007-2022	-8.8 ± 4.2	-2.0 ± 2.3	-	1.2 [0.0; 2.0]	0.021 ± 0.007	0.005 ± 0.007	-1.1

Belem region	2008-2021	-11.7 ± 5.8	-4.8 ± 2.5	-	1.4 [0.4; 1.3]	0.016 ± 0.010	-0.001 ± 0.006	-1.5
Fortaleza region	2005-2022	-16.0 ± 4.2	-2.7 ± 1.8	-	0.8 [-1.3; 2.5]	0.034 ± 0.012	0.003 ± 0.011	-0.4
Salvador region	2001-2022	-7.0 ± 4.5	-3.7 ± 1.7	-	1.9 [0.7; 3.1]	0.016 ± 0.008	0.010 ± 0.006	-1.3
South Amazon	2008-2021	0.8 ± 6.4	1.6 ± 1.8	-	-	0.005 ± 0.015	-0.003 ± 0.007	-
Midwest Brazil	2001-2022	-0.4 ± 2.1	-1.8 ± 1.1	-2.5 ± 1.9	-1.3 [-2.1; -0.3]	0.005 ± 0.003	0.005 ± 0.005	1.4
Southeast Brazil	2001-2022	-0.1 ± 4.5	-1.6 ± 1.9	-7.7 ± 8.5	-3.7 [-5.5; -1.3]	0.002 ± 0.006	0.006 ± 0.007	3.9
South Brazil	2001-2022	2.0 ± 3.8	1.1 ± 4.1	1.2 ± 1.9	-0.2 [-1.3; 0.7]	0.001 ± 0.005	-0.003 ± 0.007	0.2

326
327
328
329
330
331
332
333
334
335
336
337
338
339
340

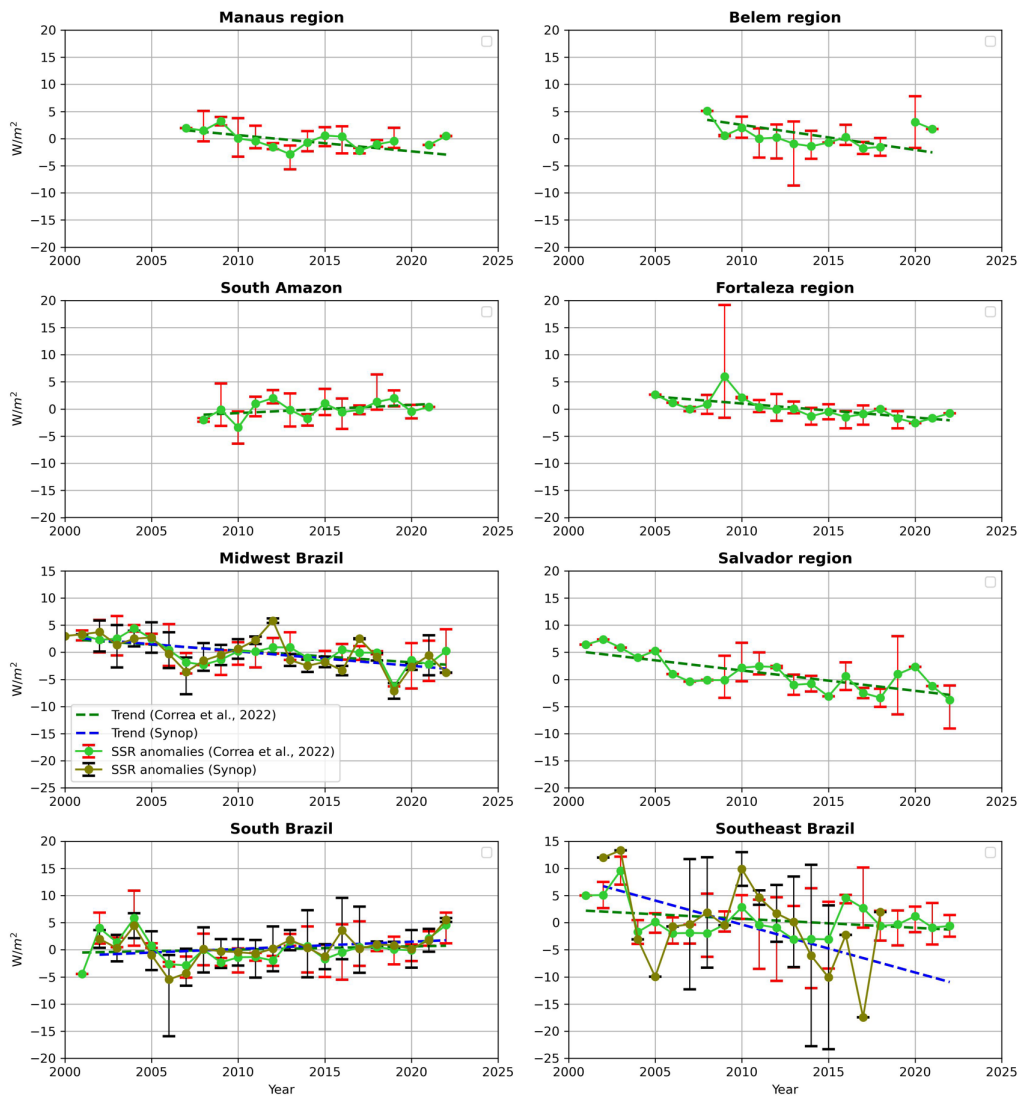
Table 1 - Trends (in W/m² per decade) for all-sky and clear-sky (using Correa et al., 2022, and using Synop cloud cover) SSR, all-sky and clear-sky (using Correa et al., 2022) fractional atmospheric absorption and Synop cloud cover at the 8 composites used in this study. Cloud Cover Radiative Effect (CCRE) referring to the Synop cloud cover trend also included. SSR trends in W/m² per decade; fractional atmospheric absorption trends in fraction (values between 0 and 1) per decade; Synop cloud cover in % per decade; and CCRE in W/m². Trends in bold are statistically significant at the 95% confidence level. Trends for Synop cloud cover were calculated using the Mann-Kendall test (see section 2.6), and as a result, the confidence interval is not always symmetrical. For this reason the confidence interval is shown in square brackets., Stations in each composite are listed in Table 32 (in appendix).

*Missing values for clear-sky Synop trends occur due to the limited amount of Synop cloud cover data (0 stations for the South Amazon composite, 2 out of 4 stations for Belem and Manaus composites) or due to not enough days flagged as clear-sky in order to generate a clear-sky time series (according to the procedure described in section 2.3).

341
342
343
344
345
346
347
348
349
350
351
352
353

The period covered by the data in this study should always be kept in mind, as it is shorter than long-term studies of SSR trends in regions like Europe, North America and China. However, this timespan should be enough to start identifying the relevant features affecting SSR on timescales of a decade and beyond. In the North and Northeast Brazil composites (Belem, Manaus, Fortaleza and Salvador ~~composites~~) statistically significant (at the 95% confidence level) negative SSR trends (dimming) were observed. In the Southeast and Middle West composites, trends were negative, although near zero and statistically insignificant. Southern Amazon and South Brazil composites both show statistically insignificant positive SSR trends (brightening). This reveals a contrasting spatial distribution of the all-sky SSR trends in the first two decades of the 21st century in Brazil: while strong dimming occurred in the northern half of the Amazon region and in the northeastern coastal region, near-zero to weak positive SSR trends occurred from the southern part of the Amazon down to the south of Brazil, including the central area of the country and the densely populated southeastern region. Figure 3 shows the time series of clear-sky SSR derived with the two methods used in the study.

354



355

356

357

358

359

360

361

362

Figure 3: Time series of clear-sky Surface Solar Radiation annual anomalies (in reference with respect to the composite full time coverage, shown in Table 1) from the eight composites used in this study. Light green time series derived using the method by Correa et al. (2022) and olive green time series derived using Synop cloud cover to identify clear-skies. The error bars indicate the maximum and minimum value for the individual stations in the respective year and composite. Trends are indicated by dashed lines.

363

364

365

366

367

368

369

370

Time series of clear-sky SSR based on synop cloud cover could not be derived in five out of the eight composites (see figure 3 and table 1). Synop clear-sky time series were derived when at least three stations in the composite had clear-sky data (see availability in table 3). The Manaus, Belem and South Amazon composites did not fulfill this requirement. In the South Amazon composite no station had Synop cloud cover available. For Belem and Manaus regions composites only two out of the four stations in each composite had Synop cloud cover data available and this limited the amount of data available to derive clear sky for the composite. For both Fortaleza and Salvador region composites, Synop cloud cover data was available for all stations, however, the few occurrences of low

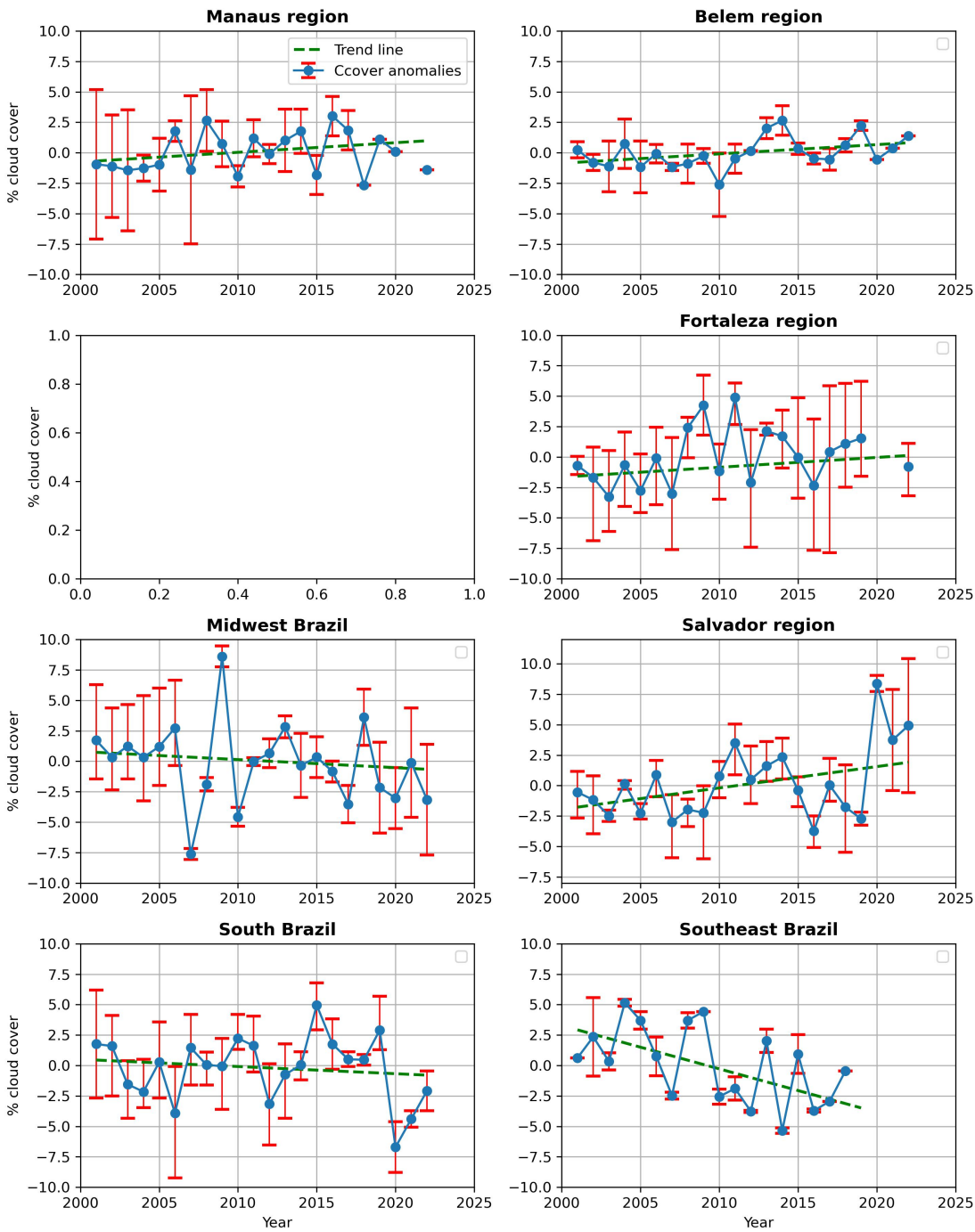
371 cloud cover days did not enable the derivation of clear-sky SSR time series following the procedure
372 described in section 2.3.

373 Clear-sky SSR time series show in general a similar pattern as observed in all-sky. All of the
374 composites show the same sign as the trends in all-sky, and six of them also indicate the same statistical
375 significance (or insignificance). The only exceptions are the Middle West and Manaus composites.
376 The former showed statistically insignificant negative trends in all-sky SSR, but statistically significant
377 negative clear-sky SSR trends. The opposite occurred in the Manaus composite: statistically significant
378 all-sky SSR trends and statistically insignificant clear-sky SSR trends. For the composites where clear-
379 sky data could be derived with both methods, in two of them (South and Midwest Brazil) both methods
380 indicate very similar inter annual variability and trends, while in the other (Southeast Brazil) the two
381 methods do not show strong agreement in the inter annual variability, but agreed in the direction of the
382 trend. Therefore, the results of the clear-sky SSR trends are supported by both clear-sky methods. These
383 results were found by both clear sky methods used in the study, although with slightly different values
384 in the trends. Regarding the magnitudes of the clear-sky SSR trends in comparison to the all-sky trends,
385 another general pattern could be observed. In all composites with statistically significant negative all-
386 sky SSR trends (Belem, Manaus, Fortaleza and Salvador), the clear-sky SSR trends showed a
387 substantially smaller magnitude. In the Southeast and Middle West, both with near-zero all-sky SSR
388 trends, the clear-sky SSR trends were both negative and of larger magnitude than their all-sky
389 counterparts. In the two composites with observed statistically insignificant all-sky SSR brightening
390 (South Amazon and South Brazil), the clear-sky SSR trends showed similar magnitudes as the all-sky
391 SSR trends.

392 These results indicate that the clear-sky processes in the atmosphere contributed to the observed
393 all-sky SSR trends in the whole of Brazil, but only in the Southern Amazon and in South Brazil their
394 magnitude might have been large enough to be able to explain the observed SSR trends. “Clear-sky
395 processes” in this context refers to the interaction between solar radiation and the components of the
396 atmosphere without the presence of clouds. Further analysis is thus needed to better understand the
397 reasons for the clear-sky and all-sky—enlighten other relevant contributors to the decadal SSR trends
398 observed in Brazil.

399 3.2 Cloud cover, AOD and water vapour trends

400 Clouds, aerosols and water vapour all can attenuate solar radiation, therefore, their variability
401 is analyzed in more details in this section. The order in which they are mentioned follow the order of
402 relevance in the discussion of solar radiation attenuation in the atmosphere, with clouds being the most
403 important aspect and water vapour the least important aspect. Figure 4 shows the SYNOP cloud cover
404 time series for 7 of the 8 composites analyzed in the study (the cloud cover time series for the Southern
405 Amazon composite could not be constructed due to too much missing data). The associated trends can
406 be found in Table 1.



408

409

410

411

412

413

Figure 4 - Time series of annual mean Synop cloud cover for seven of the eight composites used in this study. Not enough data was available to derive a time series for the South Amazon composite. The error bars indicate the maximum and minimum value for the individual stations in the respective year and composite. Trends are indicated by dashed lines.

414

415

416

417

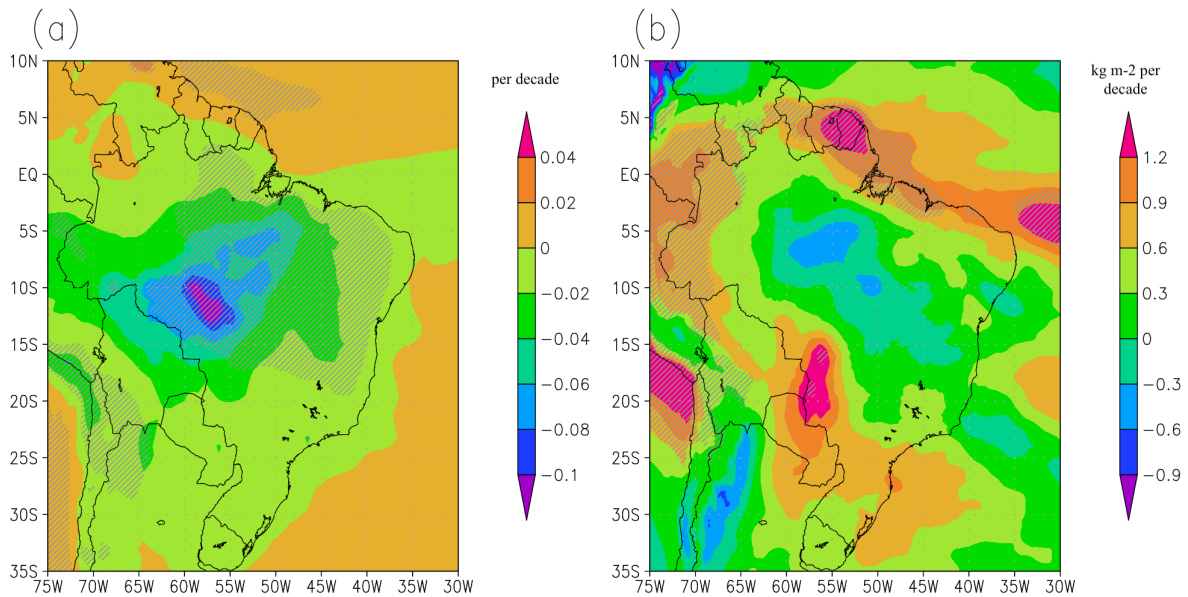
The Manaus, Belem and Southeast Brazil composites do not have synop cloud cover data for all stations (2 out of 4 available for Manaus and Belem, and 3 out of 5 for Southeast Brazil), therefore a comparison between all-sky SSR trends and Synop cloud cover at these composites is based on the assumption that the cloud cover observations for the composites are representative for all stations. This

418 is a reasonable assumption given the geographical proximity between the stations within these three
419 composites and the lack of any climatic or geographical feature that can strongly affect cloudiness at
420 individual stations (e.g. high topography). In these composites, all stations are located in areas with the
421 same precipitation regimes as classified by Ferreira and Reboita (2022), also corroborating with the
422 assumption of good representativeness.

423 Cloud cover trends are in most cases consistent in sign with the all-sky SSR trends. That is,
424 positive (negative) trends in cloud cover occurring during a period of negative (positive) SSR trends.
425 That is the case for the four composites with statistically significant all-sky SSR dimming (Belem,
426 Manaus, Fortaleza and Salvador). They all show positive trends in cloud cover, and all, except
427 Fortaleza, show statistical significance. This is consistent in the sense that the increase in cloud cover
428 contributes to the observed decrease in SSR, especially considering that the magnitude of the clear-sky
429 SSR trends at these locations was significantly smaller than the all-sky SSR trends. However,
430 quantitatively, the small magnitude of the cloud cover trends (between 0.8 and 1.9 % per decade)
431 challenges any hypothesis of a major contribution of cloud cover changes to the decadal SSR trends.
432 That is, the cloud cover trends are too small and, and as a consequence, the contribution of changes in
433 cloud cover to the SSR trends is expected to be minor. This contribution ~~the~~ is estimated objectively by
434 the CCRE (see table 1), which shows, in most cases, low values (in comparison to the all-sky SSR
435 trends), suggesting only a minor contribution from cloudiness to the SSR trends.

436 Cloud cover trends show near-zero values in the South region, suggesting no major cloud cover
437 contribution to the SSR trends. Southeast and Middle West show both statistically significant negative
438 trends in cloud cover, with remarkably strong values in SE (-3.7 [-5.5; -1.3] % per decade). Both
439 composites show near-zero but negative all-sky SSR trends, with stronger negative clear-sky SSR
440 trends. Thus, the cloud cover trends exert an opposite effect to the one of the clear-sky processes at both
441 composites. This is also consistent, in the sense that with clear-sky processes and cloud cover having
442 competing opposite effects, if their magnitude is similar, their effects cancel out, and the resulting all-
443 sky SSR trend would be near zero.

444 Figure 5 shows the decadal trend maps of annual AOD in the 2003-2020 period from CAMS
445 reanalysis and of total column water vapour in the 2001-2020 period from ERA5.



446
 447 **Figure 5 - Maps of decadal trends of (a) AOD [unitless] in the 2003-2020* period from CAMS reanalysis**
 448 **and of (b) total column water vapour [in kg m⁻²] in the 2001-2020 period from ERA5. Shaded areas indicate**
 449 **statistical significance (at the 95% confidence level).**
 450 ***The dataset was available only from 2003 onwards.**

451 In Figure 5 (a) we see a strong negative AOD trend in the Southern Amazon in the period, and
 452 slightly negative to near-zero trends in the rest of the country. Trends are statistically significant in the
 453 Southern Amazon and in the inner area of the country down to approximately 15 degrees south (shaded
 454 areas), while they lose significance towards the coast. The process that dominates the AOD trends in
 455 the Southern Amazon (and in the whole country) is the reduction of biomass burning in the Amazon
 456 region. The Southern part of the Amazon region is the area that suffers most from the biomass burning
 457 (Artaxo et al., 2006), especially in the dry season during the southern hemisphere summer/winter. A
 458 reduction in forest fires at the beginning of the 21st century has been reported (Silva Junior et al., 2021),
 459 and its effect is clear in the AOD trends. This result is consistent with the observed clear-sky SSR
 460 brightening in the Southern Amazon, but challenges the negative clear-sky SSR trends observed in most
 461 of the country. This suggests that changes in AOD were not primarily responsible for the clear-sky SSR
 462 trends in the whole of Brazil, with the exception of the Southern Amazon region.

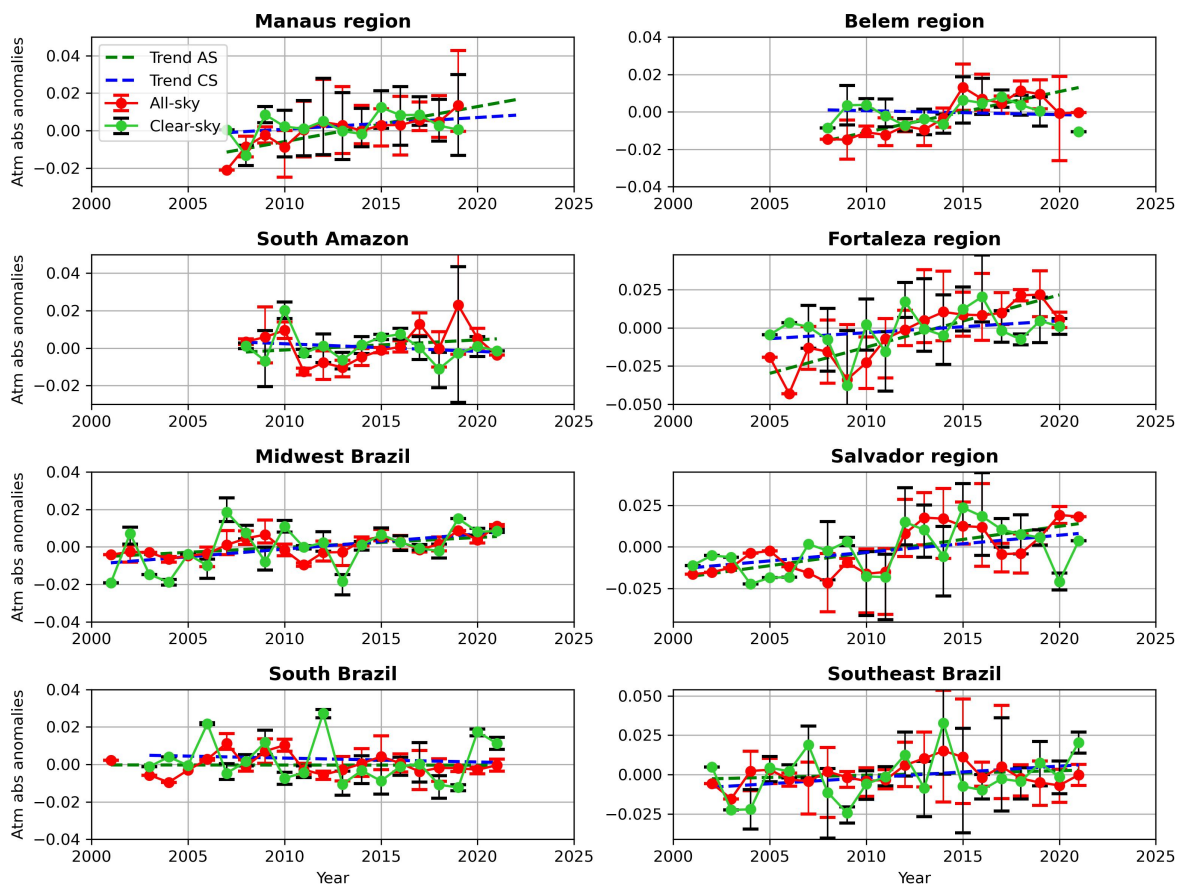
463 The water vapour trend map (Figure 5 (b)) shows remarkably negative trends in the central
 464 Amazon, in a region around the east coast of Brazil and in the southernmost part of the country.
 465 Remarkably positive trends are present from the middle Western Brazil (south of the Amazon region)

466 stretching to Southeastern Brazil, and in the northeast and north coastal regions of the country. The
 467 spatial distribution of the decadal variability of water vapour does not generally ~~fit to~~ comply with the
 468 observed clear-sky SSR trends. We used these trends to estimate the change in atmospheric clear-sky
 469 absorption due to solely water vapour, using the empirical model presented by Hakuba et al. (2016).
 470 Based on these estimations, even in a region with strong water vapour trend such as Midwest Brazil,
 471 these changes would be responsible for an increase in atmospheric clear-sky absorption (and
 472 consequently decrease in SSR) of approximately 0.4 W/m^2 per decade. This is almost one order of
 473 magnitude smaller than the clear-sky SSR trends in the region (-1.8 and -2.5 W/m^2 per decade, for
 474 clear-sky conditions based on Correa et al. (2022) and Synop cloud cover, respectively). This suggests
 475 that the water vapour contribution to the observed clear-sky SSR trends, when existed, was only minor.

476 3.3 Atmospheric absorption and Anthropogenic emissions

477 To better understand the reasons behind the observed clear-sky SSR trends and the overall
 478 processes responsible for the all-sky SSR trends, we analyzed the changes in fractional atmospheric
 479 absorption under all-sky and clear-sky conditions. Figure 6 shows these time series for the composites
 480 considered in this study both under all-sky and clear-sky conditions.

481

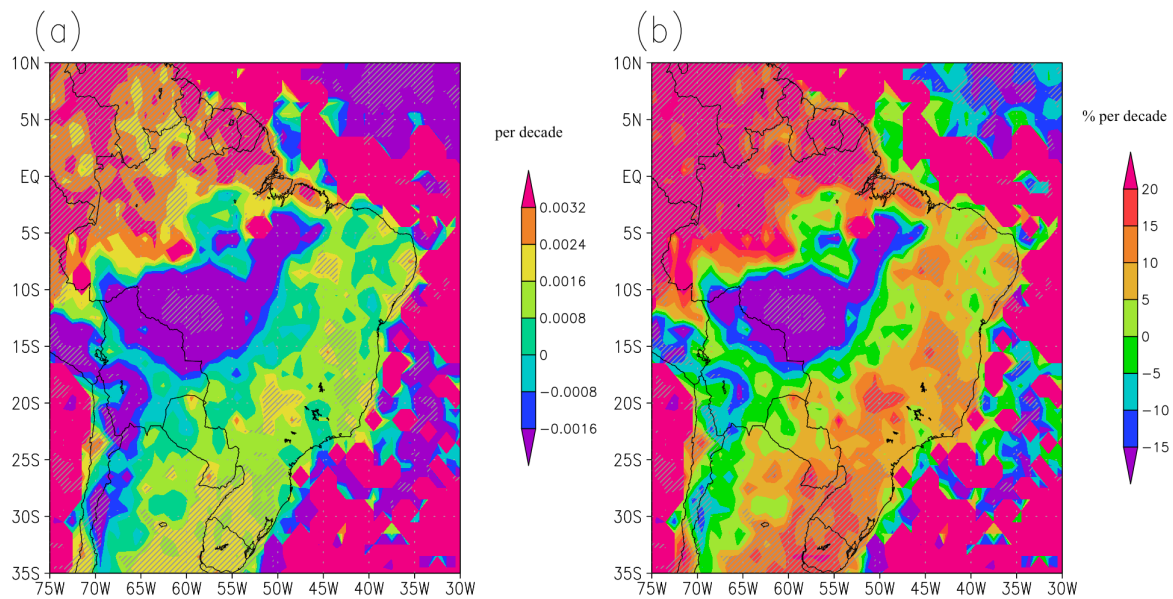


482

483 **Figure 6: Time series of all-sky (red) and clear-sky (green) fractional atmospheric column absorption**
 484 **annual anomalies for the eight composites used in this study.**

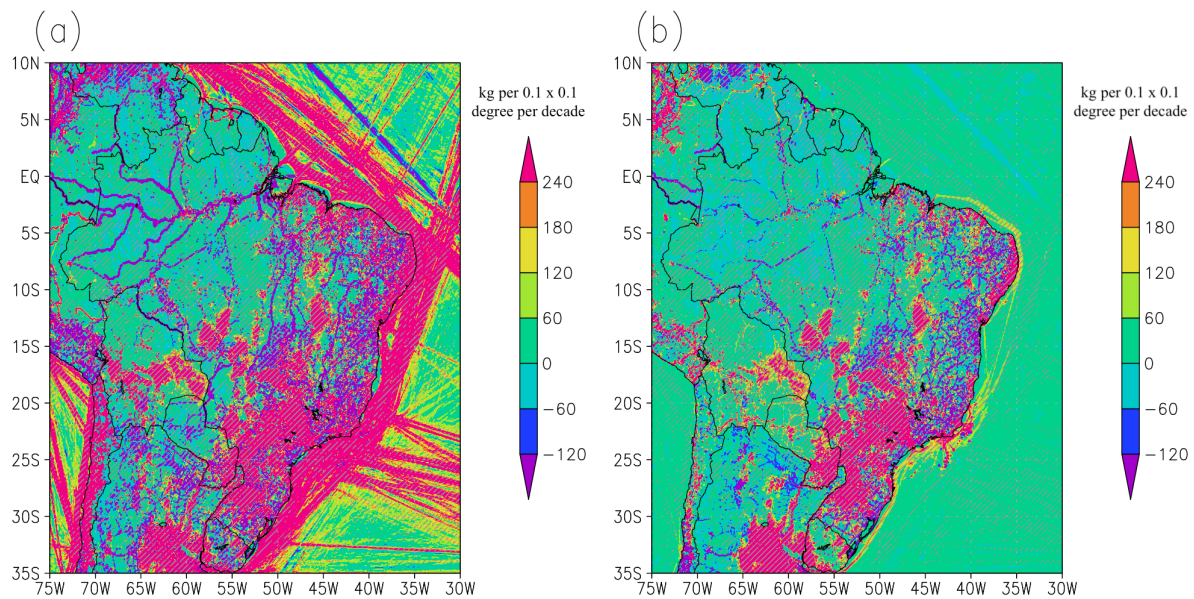
485 The fractional atmospheric absorption under all-sky conditions increased in most of the
486 composites in the first two decades of the 21st century. Five composites showed statistically significant
487 positive trends in $F_{AB_{abs}}$, they are: Manaus, Belem, Fortaleza, Salvador and Middle West. The other
488 composites also showed positive trends, but they were statistically insignificant. Under clear-sky
489 conditions, the trends are obviously smaller, as the cloud induced multiple scattering does not play a
490 role in enhancing column absorption. Only in the Salvador and Middle West composites statistically
491 significant positive trends were observed in the atmospheric absorption under clear-sky conditions. All
492 the other composites show statistically insignificant trends with the same sign as their all-sky
493 counterparts, with the exception of the South Amazon, which shows *statistically insignificant* negative
494 trends under clear-sky, contrasting to a *statistically insignificant* positive trend under all-sky conditions.

495 These results reveal two important aspects of the SSR variability in Brazil. First, in seven out
496 of the eight composites the changes in clear-sky absorption ~~fit~~ *comply with* the clear-sky SSR trends.
497 That is, increasing (decreasing) clear-sky atmospheric absorption was always linked to a decrease
498 (increase) in clear-sky SSR. Secondly, the presence of clouds greatly increased atmospheric absorption
499 (not shown) but also its trends. This has most likely happened because of the intensification of multiple
500 scattering occurring under partially cloudy skies, resulting in a magnification of the ~~effects~~ *trends* seen
501 in clear-sky conditions. This is reinforced by the fact that the strongest all-sky atmospheric absorption
502 trends were found in the four ~~cloudiest~~ composites (Manaus, Belem, Fortaleza and Salvador), which
503 happen to be the four composites with statistically significant negative all-sky SSR trends (dimming).
504 Even though these results ~~fit~~ *are consistent with* each other, they also suggest that AOD only showed
505 strong trends in the South Amazon region, and that water vapour only contributed as a minor part to the
506 observed changes in atmospheric absorption (see discussion above). Thus, this raises the question of
507 what could be the main responsible for the changes in atmospheric absorption in Brazil. To try to answer
508 this question, we analyzed the decadal trend in aerosol absorption optical depth (AAOD) at 500 nm
509 from OMI. The trend map is displayed in Figure 7.



510
 511 **Figure 7: (a) Absolute and (b) relative (%) decadal trends in Absorption Aerosol Optical Depth (AAOD)**
 512 **in the 2005-2022 period from OMI. Shaded areas indicate statistical significance (at the 95% confidence**
 513 **level).**

514 The map shows a clear distinction between the region under strong influence of the forest fires
 515 in the Amazon (South Amazon) and the rest of Brazil. In the South Amazon, the data shows a decrease
 516 in AAOD in the 2005-2022 period, while in the rest of the country an increase in absorption AAOD at
 517 500 nm is observed. The spatial distribution of the trends suggests that the reduction in AAOD in the
 518 South Amazon could be associated with the forest fires reduction also visible in the AOD trends. In the
 519 whole rest of the country, positive trends in AAOD are observed. This reveals a significant change in
 520 the optical properties of the aerosols present in Brazil in the first two decades of the 21st century, with
 521 a trend towards more absorbing aerosols (at 500 nm) in most of the country. The AOD trend map
 522 (Figure 5a) shows that in the same areas where AAOD increases, AOD remains nearly constant, with
 523 trends close to zero. In order to better visualize potential reasons for an increase in AAOD at 500 nm
 524 in most of Brazil, we also ~~verified~~ *investigated* trends in anthropogenic SO₂ and Black Carbon emissions
 525 in Brazil. They are displayed in Figure 8.



526
 527 **Figure 8: Decadal trends of annual mean (a) SO₂ and (b) Black Carbon anthropogenic emissions (in kg per**
 528 **0.1x0.1 degree grid per decade) for the 2001-2018 period from EDGAR. Shaded areas indicate statistical**
 529 **significance (at the 95% confidence level).**

530 They show a general increase in anthropogenic emissions in most of Brazil, especially in highly
 531 populated areas. The only areas not showing increase in anthropogenic emissions are in the Amazon
 532 rainforest. This might be counterintuitive when comparing the emissions trends (figure 8) with AOD
 533 trends (figure 5a), as the strongest AOD trend is observed in the south of the Amazon region. However,
 534 EDGAR emission estimates do not consider large scale biomass burning, land use change and forestry
 535 (Crippa et al., 2018). As discussed in section 3.2, the AOD negative trend is mostly associated with
 536 reductions in biomass burning in the first two decades of the 21st century in the Amazon. Therefore,
 537 the biggest cause of the AOD trend (Figure 5a) is not considered in the emission data used in Figure 8.

538 Even though, according to figure 8, anthropogenic emissions did not increase significantly in
 539 the Amazon region, emissions still increased around the biggest cities in the region, like Manaus and
 540 Belem. This is of special relevance for this study, since seven of the eight composites are centered
 541 around cities with over a million inhabitants, where the large and usually increasing population (Lobo
 542 and Cunha, 2019) plays an important role to the atmospheric composition. The only composite that
 543 does not follow this rule is the South Amazon composite, where the biggest city is Porto Velho, which
 544 in 2020 had a population of less than 500'000 people (IBGE 2022). As anthropogenically emitted
 545 aerosols tend to account for a larger fraction of solar radiation absorption than natural aerosols (Wang

546 et al., 2009), this increase in anthropogenic emissions (especially of black carbon) ~~fits to~~ **complies with**
547 the increasing AAOD in most of Brazil. Even though sulphate aerosols absorb much less shortwave
548 radiation than black carbon, the increasing presence of scattering aerosols can also have a similar effect
549 to the presence of broken clouds for atmospheric absorption (as discussed for the composites in North
550 and Northeast Brazil): they increase multiple scattering, increasing the optical path of the photons,
551 which increases the chances for absorption by the atmosphere. Therefore, the increasing anthropogenic
552 emissions **complies with** ~~fit to~~ the observed increase in atmospheric absorption in most of Brazil in the
553 period of study. Similar results indicating a stronger impact of the changes in optical properties of the
554 aerosols than the changes in aerosol optical depth on the observed SSR trends were also found for Japan
555 in the 1990s by Kudo et al. (2012).

556 4. Discussion

557 4.1 Physical consistency of the results

558 The results of this study point to a relevant impact of changes in atmospheric absorption in at
559 least half of the regions analyzed. However, this is based on the fractional atmospheric absorption data,
560 which is derived (as described in section 2.4) by combining in situ SSR (point) measurements with
561 gridded data of surface albedo and outgoing shortwave radiation at TOA, at 0.25 and 1.0 degree spatial
562 resolution, respectively. So the first question to be addressed is whether these results can be trusted
563 even with the use of different spatial resolutions. Schwarz et al. (2018) investigated the spatial
564 representativeness of SSR measurements in many stations around the world, including four stations in
565 Brazil: Florianopolis, São Martinho da Serra (both in South Brazil), Brasilia (in Middle West) and
566 Petrolina (~ 450 km away from Salvador). The authors found a good representativity of SSR for the 1-
567 degree surroundings at most stations around the world at the monthly time scales, with estimated
568 decorrelation lengths (**the distance over which a point measurement is representative**) always higher
569 than 3 degrees in all of the four Brazilian locations. Madhavan et al. (2017) investigated spatial
570 representativeness of SSR measurements at shorter time scales, and found that point measurements
571 were representative to a 10 x 10 km area in time scales up to around one hour (from 26 minutes at
572 overcast conditions to 70 minutes at broken clouds conditions). The authors demonstrated that the
573 decorrelation lengths (~~the point measurement is representative~~) increase linearly (on a log-log scale)
574 with decreasing frequency (longer time ~~time~~ averaging). Following the results of the study by
575 Madhavan et al. (2017), this would lead to decorrelation lengths around the order of 100 km (~1 degree)
576 at the daily (24-hour) time scales. Therefore, based on the interpretation of these results, we can expect
577 a satisfactory consistency in the results from combining point measurements at the surface with 1-
578 degree measurements at the TOA at daily time scales, as done in this study. An in-depth analysis to
579 estimate the decorrelation lengths at daily time scales of each station goes beyond the scope of the
580 study.

581 The performance of the gridded products used in this study are discussed in their
 582 respective documentations, referenced in section 2. Spectral surface albedo is reported as a main source
 583 of uncertainty in the satellite based products, especially OMI AAOD, however, this tends to be a major
 584 problem over the ocean. Sub-grid cloud contamination tends to also represent a problem for the retrieval
 585 of satellite based products. But this is reported to lead to an over/under estimation of the average AAOD,
 586 but should not affect the representation of its long-term variability. No issues with the long-term
 587 variability of the reanalysis products were reported.

588 ~~Also~~ Regarding atmospheric absorption, previous studies (e.g. Li et al., 1995; Byrne et al.,
 589 1996) have shown an enhancement in atmospheric absorption under cloudy conditions. According to
 590 previous literature, such an enhancement would not be caused by cloud absorption, but by cloud
 591 scattering, which increases the optical path of a photon in the atmosphere, consequently increasing the
 592 chances of this photon to be absorbed by other components of the atmosphere, such as water vapour
 593 and aerosols. Even though the existence of this mechanism is clear, the quantitative influence this could
 594 have on the energy budget at any location would also depend on the characteristics of cloud occurrence
 595 (e.g. the frequency of cloud free, overcast and partially cloudy conditions). As much as cloud free
 596 conditions are not optimal for atmospheric absorption, completely overcast conditions are not either.
 597 Under fully cloudy conditions, the backscattering of incoming shortwave radiation is high, usually not
 598 increasing the optical path of the photons and not allowing them to reach lower levels of the atmosphere,
 599 where water vapour and aerosol concentrations are higher. Thus, the high occurrence of partially cloudy
 600 conditions would ~~optimise~~ ~~increase~~ the cloud effects on atmospheric absorption, ~~via the increase in the~~
 601 ~~optical path of the photons. Under such conditions scattering by clouds can increase the optical path of~~
 602 ~~the photons, while still allowing a significant fraction of them to reach the lowest levels in the~~
 603 ~~atmosphere, where water vapour and aerosol concentrations are the highest.~~ Such conditions are found
 604 in Belem, Manaus, Fortaleza and Salvador, due to the importance of local convection for cloud
 605 formation in such hot and humid locations. The differences in the fractional atmospheric absorption
 606 trends between clear-sky and all-sky conditions at these locations reinforces this: trends under all-sky
 607 conditions are one order of magnitude larger than their clear-sky counterparts. This is not observed at
 608 all the other locations, which ~~have a higher dependence~~ ~~are much more dependent~~ on mesoscale and
 609 synoptic scale ~~phenomena~~ ~~for cloud formation than the previously mentioned locations.~~ In fact, a
 610 difference in the precipitation regimes between the region where all the four above-mentioned
 611 composites are located and the rest of Brazil has already been pointed out by Reboita et al. (2010) and
 612 by Ferreira and Reboita (2022).

613 Chtirkova et al. (2023) investigated the potential effect of internal variability on the SSR trends,
 614 and the relevance especially of Atlantic oceanic modes like the Atlantic Meridional Mode (AMM) or
 615 the Atlantic Multidecadal Oscillation (AMO) to affect SSR trends by changing cloudiness in Brazil.
 616 The AMM and AMO went to lower values during the period of study (2001-2022), which should lead
 617 to decreasing SSR in Northeastern Brazil. This ~~fits~~ ~~is consistent with~~ ~~to~~ the negative SSR trends in the

618 region. But it is important to note that this reduction in the oceanic modes values did not represent a
 619 major phase transitions of these modes. A major increase in AMO occurred in the 1990s, and the cloud
 620 cover trends (from ERA5) for the 1990-2006 period show a strong decrease in cloud cover in most of
 621 Brazil, especially the south and western part of the country. No SSR data was available for further
 622 investigation in this study, but the importance of internal variability for SSR trends should not be
 623 neglected in future studies

624

625 The trends in SSR and supporting information in the eight composites made it possible to
 626 separate the discussion of the causes for the SSR trends into three groups. **The composites in each group
 627 and their common characteristics are listed on table 2.**

Composites	Common characteristics
Manaus, Belem, Fortaleza and Salvador	Strong all-sky dimming
	Distinguished clear-sky dimming with lower magnitude than the all-sky
	Positive cloud cover trends
	Positive trends in all-sky atmospheric absorption
	Positive trends in clear-sky atmospheric absorption, but one order of magnitude smaller than their all-sky counterparts (this item does not apply to Salvador)
Southeast Brazil and Midwest Brazil	Strong negative cloud cover trends
	Negative clear-sky SSR trends
	Negative and statistically insignificant SSR trends
South Amazon and South Brazil	Statistically insignificant all-sky brightening
	Statistically insignificant clear-sky brightening

628

629 **Table 2: Groups of composites with and their common characteristics as indicated by the results**
 630 **presented in this study.**

631 Based on this, we separated the discussion on the causes for SSR trends in three sections, each
 632 discussing one of the three groups. ~~The first group is composed of the four composites in the north and~~
 633 ~~northeast Brazil (Manaus, Belem, Fortaleza and Salvador). Five characteristics were observed in all of~~
 634 ~~these locations: 1. strong all sky SSR dimming; 2. distinguished clear sky dimming with lower~~
 635 ~~magnitude than the all sky; 3. Positive cloud cover trends; 4. Positive trends in all sky atmospheric~~
 636 ~~absorption; and 5. positive trends in clear sky atmospheric absorption but one order of magnitude~~
 637 ~~smaller than their all sky counterparts. The second group is composed of the Southeast Brazil and~~

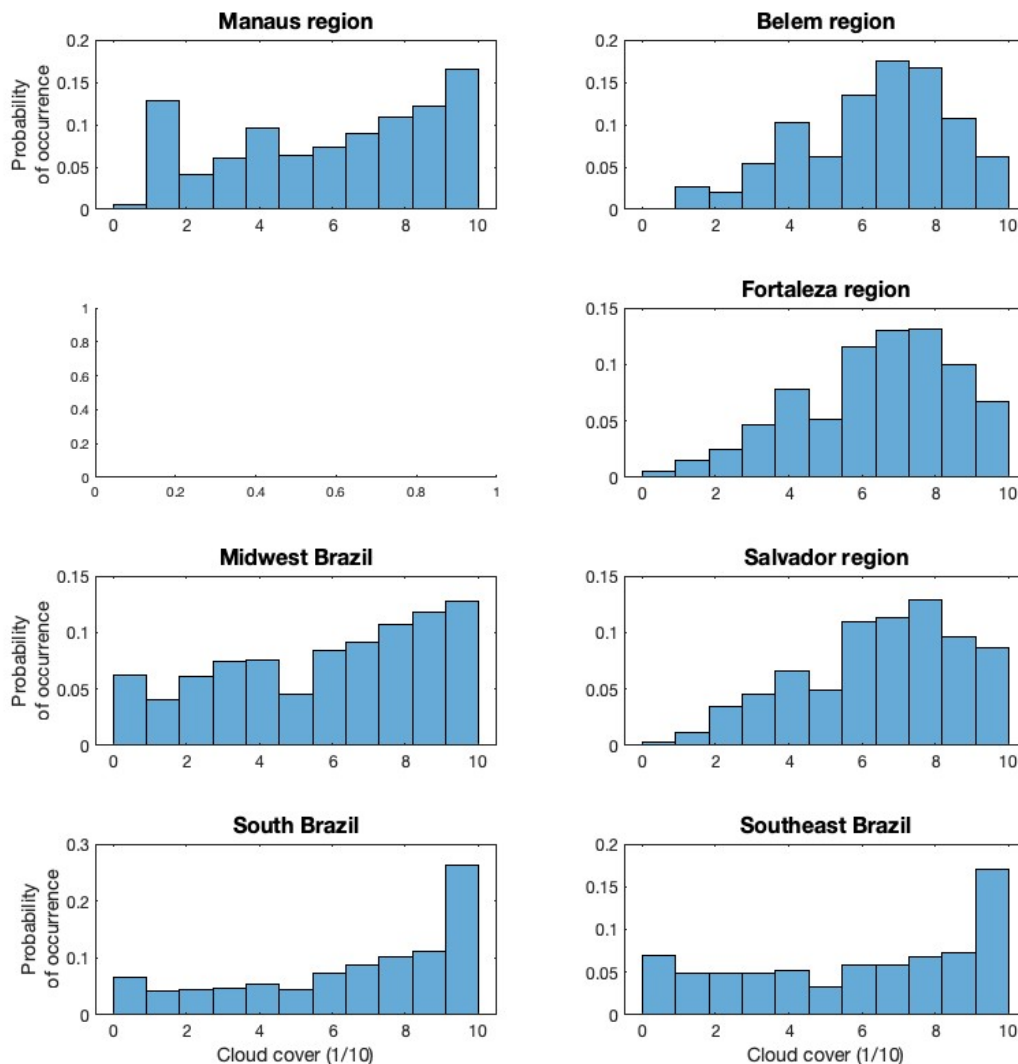
638 ~~Middle West Brazil composites. Both of these composites showed: 1. Strong negative cloud cover~~
 639 ~~trends; 2. negative clear sky SSR trends; and 3. negative and statistically insignificant SSR trends. The~~
 640 ~~third group, composed by the South Amazon and South Brazil composites show: 1. Statistically~~
 641 ~~insignificant all sky brightening; and 2. statistically insignificant clear sky brightening. Based on this,~~
 642 ~~we separated the discussion on the causes for SSR trends in three sections, each discussing one of the~~
 643 ~~three groups.~~

644 4.2 Dimming in North and Northeastern Brazil

645 In this section, we discuss the dimming observed in the Manaus, Belem, Fortaleza and Salvador
 646 composites, located in North and Northeastern Brazil. All of the composites showed statistically
 647 significant all-sky dimming in the period, associated with a clear-sky dimming which was statistically
 648 significant in all composites, except Manaus. The difference in the magnitude of the all-sky SSR trends
 649 (from -6.3 W/m^2 per decade in Salvador to -18.8 W/m^2 per decade in Fortaleza) to the clear-sky SSR
 650 trends (from -2.0 W/m^2 per decade in Manaus to -4.8 W/m^2 per decade in Belem) in the four composites
 651 suggests that the clear-sky processes alone are unlikely to be strong enough to explain the SSR trends
 652 in these locations. However, the fact that the clear-sky trends show the same sign as the all-sky trends,
 653 with (in most cases) statistical significance, indicates that processes ~~visible~~ occurring under clear-skies
 654 did contribute significantly to the overall trends. The contrast between all-sky and clear-sky also
 655 indicates a potential contribution of changes in cloud cover to the trends. In fact, we identified positive
 656 cloud cover trends, consistent with the observed reduction in SSR, but the magnitude of the trends (from
 657 0.8% per decade in Fortaleza to 1.9% per decade in Salvador) and the resulting impact of these cloud
 658 cover trends on the SSR trends, estimated by the CCRE (see Table 1), is small when compared to the
 659 SSR trends. Thus, our results (summarised in the table 1) suggest contributions from both clear-sky
 660 processes and cloud cover to the SSR trends, but none of them show a remarkable dominance compared
 661 to the other.

662 Further analysis of the atmospheric absorption showed strong positive (and statistically
 663 significant) trends in atmospheric absorption in all four composites. We also found that the atmospheric
 664 absorption trends were greatly enhanced by the presence of clouds. This happens because the scattering
 665 by clouds increases the optical path of the photons. This effect ~~is especially remarkable~~ occurs primarily
 666 under broken clouds conditions, when three-dimensional multiple scattering magnifies this effect. Our
 667 findings ~~fit~~ comply with the results presented by Byrne et al. (1996) and references therein, which
 668 highlight the enhancement of atmospheric absorption of solar radiation under broken clouds conditions.
 669 Results from Li et al. (1995) also suggested that this effect is stronger in tropical regions, and the authors
 670 discuss that this is associated primarily aerosol and water vapour absorption rather than cloud
 671 absorption. The characteristics of the distribution of cloudiness in the four composites, displayed in
 672 Figure 9, might also play a role in this process. Stations from these composites tend to have frequent
 673 occurrences of partially cloudy conditions. In the Belem, Fortaleza and Salvador composites the daily

674 cloud cover is between 25% and 80% in around two thirds of the days. For the Manaus and Midwest
 675 Brazil composites this range of cloud cover occurred in around half of the days and for South and
 676 Southeast Brazil composites this value is around one third. Thus, at the daily scale we see a dominance
 677 of partially cloudy occurrences at three out of the four composites discussed in this section. Even though
 678 the same distinguishable characteristic was not found for the Manaus composite at the daily scale, based
 679 on the regionalization of precipitation regimes by Reboita et al. (2010), we would expect the same
 680 finding at a more refined time scale also for the Manaus composite. That would be the expectation
 681 because of the higher relevance of local convection at hot and humid locations (convective clouds cause
 682 more broken cloud fields than large scale synoptic clouds) -ast the four composites discussed in this
 683 section, in comparison to the other composites, where mesoscale and synoptic meteorological systems
 684 tend to play a more important role for cloud formation. This higher occurrence of broken clouds in the
 685 regions of the four composites discussed in this section then tends to play an important role for the
 686 enhancement of atmospheric absorption.



687
 688

689 **Figure 9: Distribution of daily Synop cloud cover occurrences in seven out of the eight composites used in**
690 **this study. Not enough data was available to derive a distribution for the South Amazon composite.**

691 A simple multiplication between the incoming TOA radiation at each composite and the trends
692 in fractional all-sky atmospheric absorption (shown in Table 1) reveals an estimated increase in all-sky
693 atmospheric absorption from approximately $6 \pm 3 \text{ W/m}^2$ per decade in Belem up to $14 \pm 5 \text{ W/m}^2$ per
694 decade in Fortaleza. If we assume that such an increase in atmospheric absorption is directly reflected
695 in a reduction in SSR, we find that the effect of changes in atmospheric absorption under all-sky
696 conditions have a higher effect than the estimated clear-sky SSR trends (see table 1) and the estimated
697 effects of changes in clouds cover (see CCRE in table 1), and are more consistent with the magnitude
698 of the observed all-sky SSR trends (presented in table 1). Thus, these results suggest that the increase
699 in atmospheric absorption was the strongest contributor for the negative SSR trends observed in these
700 four composites in north and northeast Brazil, with contributions also from changes in cloud cover. The
701 difference in the all-sky and clear-sky absorption trends at these four composites indicates that clouds
702 played an important role in the increasing in absorption, most likely by enhancing the optical path of
703 photons via multiple scattering under partially cloudy conditions. The results also suggest that these
704 changes in atmospheric absorption were greatly influenced by the changes in the optical properties of
705 the aerosols present in these regions. Our results showed the occurrence of increasing anthropogenic
706 emissions of SO_2 and black carbon, which did not seem to significantly change the AOD (possibly
707 because of its competing effects with the reduction of biomass burning emissions in South Amazon),
708 but increased the AAOD. This is most likely the cause for the increase in atmospheric absorption at the
709 four composites. All of this points to a relevant influence of anthropogenic factors to the SSR trends in
710 the first two decades of the 21st century in the regions around Manaus, Belem, Fortaleza and Salvador.
711 Remembering that these are all big cities with over a million inhabitants each, therefore this result could
712 be biased towards big population centers.

713 4.3 Midwest and Southeast Brazil

714 In this section we discuss the causes of the decadal SSR trends in the Middle West and
715 Southeast Brazil composites. Both all-sky SSR composites show near-zero trends, with $-0.4 \pm 2.7 \text{ W/m}^2$
716 per decade in the Middle West and $-0.6 \pm 5.4 \text{ W/m}^2$ per decade in Southeast Brazil in the first two
717 decades of the 21st century. Both composites show clear-sky SSR dimming (statistically significant in
718 the Middle West and statistically insignificant in the Southeast) and statistically significant decrease in
719 cloud cover in the period. An increase in atmospheric absorption was also observed at these locations,
720 but the trends were substantially smaller than the trends observed in the four composites discussed in
721 the previous section. These results already suggest different physical processes playing a role in the
722 causes of SSR decadal trends in these regions.

723 The trends in fractional clear-sky atmospheric absorption in the two composites are similar to
724 each other (0.0051 ± 0.005 per decade in the Middle West and 0.0059 ± 0.007 per decade in the

725 Southeast) and are larger than the trends in three out of the four composites discussed in the previous
726 section. The clear-sky absorption trends are also larger than the all-sky absorption trends in the Middle
727 West and Southeast. This indicates a bigger relative relevance of the cloud-free processes for the SSR
728 trends in these two regions compared to the four locations previously discussed. This is reinforced by
729 the clear-sky SSR dimming at the two locations, and is also most likely associated with increasing
730 anthropogenic emissions, which lead to more absorptive aerosols, without significant change in AOD.

731 A comparison between the results of these two composites with the four composites in North
732 and Northeast Brazil supports the discussion regarding the impacts of broken clouds to the solar
733 atmospheric absorption and the distribution of cloud cover occurrences, presented in the previous
734 section. As discussed by Reboita et al. (2010) and by Ferreira and Reboita (2022), in the region from
735 Middle West to Southeastern Brazil a stronger influence of large scale synoptic meteorological systems
736 like cold fronts, South Atlantic Convergence Zone (SACZ) and the South American Low Level Jet
737 (SALLJ) contrasts with Northern and Northeastern Brazil, where local convection and circulation play
738 a more important role. This leads to different precipitation and cloudiness regimes between the
739 composites discussed in this section and in previous section. These regimes magnify the effects of
740 atmospheric absorption in the North and Northeastern Brazil, again fitting to the results by Li et al.
741 (1995), while not doing so in the rest of the country.

742 The results of these two composites also show a significant positive effect of changes in cloud
743 cover on the SSR trends. Strong significant negative trends in cloud cover were observed at both
744 regions. As a result of the competing effects between cloud-free processes and changes in cloud cover,
745 the resulting SSR trends in the first two decades of the 21st century were negative, but near-zero, for
746 both composites. This shows opposing effects of anthropogenic (changes in aerosols) and natural
747 (changes in cloud cover) changes canceling out.

748 **4.4 South Amazon and South Brazil**

749 In this section we discuss the causes for the SSR decadal trends in the South Amazon and South
750 Brazil. In both regions statistically insignificant brightening was observed in the all-sky SSR trends.
751 Clear-sky SSR trends also showed brightening (statistically insignificant) in both regions. Cloud cover
752 trends in South Brazil were rather small (-0.4 [-1.4; 0.6] % per decade), while cloud data was not
753 available for South Amazon.

754 For the South Amazon, the most relevant aspect to be discussed is the strong negative trend in
755 AOD observed in the study period, associated with the documented reduction in deforestation and
756 biomass burning in the Amazon (Silva Junior et al., 2021). Amazon biomass burning aerosols play an
757 important role in the atmospheric transmissivity in the region, but their emission, and consequently their
758 effects, are highly seasonally dependent, as shown by Schwarz et al. (2019). For this reason, even
759 though the annual AOD decadal trends show very strong negative values, the strong effects on SSR are
760 present mostly in the dry season (southern hemisphere winter), and are smoothed out with annual means

761 and decadal trends calculations. The seasonal clear-sky SSR trends in this composite are positive
762 (statistically insignificant at the 95% confidence level) in winter and spring (5.0 ± 5.6 and 1.1 ± 3.9
763 W/m^2 per decade, respectively) and negative (statistically insignificant at the 95% confidence level) in
764 summer and fall (-2.6 ± 2.7 and -1.6 ± 3.3 W/m^2 per decade, respectively), reinforcing this hypothesis.
765 This smoothing of the AOD effects in the annual means and decadal trends is most likely the reason
766 why, despite the strong negative AOD trends in the region, the all-sky and clear-sky SSR trends show
767 positive trends with an absolute magnitude remarkably smaller than the trends observed in north and
768 northeastern Brazil. This counterintuitive result (strong negative AOD decadal trend not resulting in
769 strong brightening neither in all-sky nor in clear-sky SSR) reveals the importance of taking seasonality
770 into account when investigating the response of SSR to changes in AOD.

771 In South Brazil, the SSR decadal trends are weakly positive, not of statistical significance, both
772 under all-sky and clear-sky conditions. This suggests the lack of a strong driver for the SSR trends in
773 the period analyzed. Cloud cover shows a small negative trend (statistically insignificant). Near-zero
774 trends are also found in AOD and in atmospheric absorption. The map of AAOD at 500 nm shows small
775 positive trends in the period, but water vapour shows small negative trends. It is important to note that
776 due to the logarithmic response of atmospheric absorption to changes in water vapour (e.g. Hakuba et
777 al., 2016), this is the region in Brazil with the expected strongest sensitivity to changes in water vapour.
778 Combining all these results together denotes competing small effects from different sources, and this is
779 most likely the reason for the resulting non significant trend observed. Another relevant aspect to be
780 highlighted, is that the period of analysis did not show a strong transition in the signal from oceanic
781 modes in the Atlantic. Chtirkova et al. (2023) pointed out the importance of the AMM and AMO
782 oceanic modes for the SSR trends in South America. This could be relevant for all composites, but the
783 lack of strong effects on SSR changes of the existing forcing elements in South Brazil in the post 2000
784 period let us to hypothesize that in a transitional period of AMM and/or AMO, internal variability could
785 dominate the SSR trends in this region, especially via changes in cloud cover. This hypothesis is
786 reinforced by the cloud cover trends from ERA5 for the 1990-2006 period (Figure A1, in appendix),
787 which show strong negative cloud cover trends in the region associated with the transitioning of the
788 AMO from a negative to a positive phase. The expectation is that the cloud cover trends in this period
789 dominated the SSR trends, causing brightening in the last decade of the 20st century in South Brazil.
790 However, the lack of SSR data before 2000 did not allow us to verify this hypothesis.

791 5. Conclusions

792 In this study we presented and investigated the magnitudes of the SSR trends and their
793 associated causes over the first two decades of the 21st century based on 34 stations in Brazil, divided
794 into 8 composites of 3 to 5 stations each. These are: Manaus region, Belem region, South Amazon,
795 Fortaleza region, Middle west, Salvador region, Southeast Brazil and South Brazil. The exact temporal

796 coverage of the SSR time series was composite-dependent, covering 22 years (2001-2022) in the four
797 southernmost composites (South, Southeast, Middle West and Salvador), and only 14 years (2008-
798 2021) in the South Amazon composite, the shortest time span of all composites in this study. *The*
799 *limited length of the periods should be kept in mind, as they are shorter than the long-term*
800 *dimming/brightening studies performed in regions like Europe.* -We used cloud cover data from in situ
801 measurements, clear-sky time series derived with two different methods (using Synop cloud cover and
802 using the method by Correa et al., 2022), atmospheric absorption calculated combining in situ and
803 satellite measurements, AOD from the CAMS reanalysis, AAOD from OMI satellite observations and
804 anthropogenic emissions from EDGAR to investigate the causes of the SSR trends in the eight
805 composites in their period of data availability. Our results showed that a strong dimming occurred in
806 the composites located in north and northeast Brazil (Manaus, Belem, Fortaleza and Salvador) in the
807 period of study, while the other four composites all showed statistically insignificant trends (positive in
808 the South Amazon and South Brazil, and negative in the Southeast and Midwest). A deeper analysis on
809 the causes of the trends revealed significant contributions of both clear-sky and cloud cover changes to
810 the trends observed in the north and northeast Brazil, but with a dominance of the effects of increasing
811 atmospheric absorption under all-sky conditions. Previous studies (e.g, Li et al., 1995; Byrne et al.,
812 1996) have discussed the increase in atmospheric absorption under broken cloud conditions due to the
813 multiple scattering by clouds and absorption by water vapour and aerosols. In the case of north and
814 northeast Brazil, we believe that this is associated with an increase in absorption possibly by aerosols,
815 also responsible for a clear-sky SSR dimming, and the characteristics of cloud occurrence in those
816 regions. The massive occurrence of partially cloudy conditions at these regions, in comparison with the
817 other composites analysed in this study, make this mechanism much more relevant at the North and
818 Northeast Brazil stations than in all of the others. In Southeast and Middle West Brazil, statistically
819 insignificant negative SSR trends in the period were most likely the results of competing effects of
820 negative cloud cover trends (resulting in a positive forcing on all-sky SSR) and negative clear-sky SSR
821 trends (resulting in a negative forcing on all-sky SSR), where the clear-sky trends are also most likely
822 associated with changes in aerosol absorption. In the South Amazon the signal of the strong aerosol
823 reduction, resulting from the reduction in biomass burning in the Amazon at the beginning of the 21st
824 century (Silva Junior et al., 2021), dominated the observed brightening. *But the resulting SSR trend*
825 *was not statistically significant. A potential reason for this might be the strong seasonality of the*
826 *biomass burning in the Amazon (Schwarz et al., 2019), which means that the strong changes in AOD*
827 *are affecting SSR only a few months per year. Due to missing data we were not able to assess the extent*
828 *of cloud cover contribution to this result*~~*due to the strong seasonality of the biomass burning in the*~~
829 ~~*Amazon (Schwarz et al., 2019), the resulting trend was statistically insignificant.*~~ Finally in South
830 Brazil, competing minor effects of cloud-free processes and cloud cover changes resulted in statistically
831 insignificant brightening. This study contributes to the understanding of the causes of SSR decadal

832 trends in a world region with still limited observational data, and opens space for further research on
833 the climate effects of such trends.

834 **Data availability**

835 The data from the IAG/USP station can be requested at
836 http://www.estacao.iag.usp.br/sol_dados.php (last access: 21 Feb 2024). The data from
837 INMET stations can be requested at <https://bdmep.inmet.gov.br/> (last access: 21 Feb 2024).
838 The BSRN SSR data is available at the BSRN website (<https://bsrn.awi.de/>). The CERES
839 products are available at the CERES website (<https://ceres.larc.nasa.gov/data/>). The ERA5
840 reanalysis data used in this study is available under
841 [https://cds.climate.copernicus.eu/cdsapp#!/dataset/reanalysis-era5-single-levels-monthly-](https://cds.climate.copernicus.eu/cdsapp#!/dataset/reanalysis-era5-single-levels-monthly-means)
842 [means](https://cds.climate.copernicus.eu/cdsapp#!/dataset/reanalysis-era5-single-levels-monthly-means) . The CAMS AOD reanalysis data is available under
843 <https://www.ecmwf.int/en/research/climate-reanalysis/cams-reanalysis> . Data of
844 anthropogenic emissions estimates is available at the EDGAR website
845 (https://edgar.jrc.ec.europa.eu/emissions_data_and_maps , last access: 21 Feb 2024). The data
846 from the OMI instrument used in this study is available at
847 https://disc.gsfc.nasa.gov/datasets/OMAERUVd_003/summary (last access 21 Feb 2024). The
848 satellite cloud fraction data from CLARA, used to apply the clear-sky method used in this
849 study, can be found on the CM SAF website (<https://www.cmsaf.eu/>) and downloaded using
850 the Web User Interface at <https://wui.cmsaf.eu/>

851 **Author contributions**

852 LFC designed the study, organised the data and wrote the original manuscript. DF, BC and MW revised
853 and edited the text. All authors contributed to the analysis and to the final paper.

854 **Competing interests**

855 The authors declare that they have no conflict of interest.

856 **Acknowledgements**

857 This study was funded by the Swiss National Science Foundation grant no. 200020_188601.
858 The authors would like to thank the Instituto Nacional de Meteorologia (INMET) and the Weather
859 Station of the Institute of Astronomy, Geophysics and Atmospheric Science of the University of São
860 Paulo for providing the meteorological observations. We express our gratitude to the teams that produce
861 and maintain the high quality meteorological data used in this study, from BSRN, CERES, ERA5,
862 CAMS, OMI, EDGAR and CLARA.

863 **References**

864 Artaxo, P., Oliveira, P. H., Lara, L. L., Pauliquevis, T. M., Rizzo, L. V., Junior, C. P., ... &
865 Correia, A. L. (2006). Efeitos climáticos de partículas de aerossóis biogênicos e

- 866 emitidos em queimadas na Amazônia. *Revista brasileira de meteorologia*, 21(3a),
867 168-22.
- 868 Augustine, J. A., & Capotondi, A. (2022). Forcing for multidecadal surface solar radiation
869 trends over Northern Hemisphere continents. *Journal of Geophysical Research:*
870 *Atmospheres*, 127(16), e2021JD036342.
- 871 Byrne, R. N., Somerville, R. C. J., & Subařilar, B. (1996). Broken-cloud enhancement of
872 solar radiation absorption. *Journal of Atmospheric Sciences*, 53(6), 878-886.
- 873 Chiacchio, M., & Wild, M. (2010). Influence of NAO and clouds on long-term seasonal
874 variations of surface solar radiation in Europe. *Journal of Geophysical Research:*
875 *Atmospheres*, 115(D10).
- 876 Chtirkova, B., Folini, D., Correa, L. F., & Wild, M. (2023). Internal variability of the climate
877 system mirrored in decadal-scale trends of surface solar radiation. *Journal of*
878 *Geophysical Research: Atmospheres*, e2023JD038573.
- 879 Correa, L. F., Folini, D., Chtirkova, B., & Wild, M. (2022). A Method for Clear-Sky
880 Identification and Long-Term Trends Assessment Using Daily Surface Solar
881 Radiation Records. *Earth and Space Science*, 9(8), e2021EA002197.
- 882 Crippa, M., Guizzardi, D., Muntean, M., Schaaf, E., Dentener, F., Van Aardenne, J. A., ... &
883 Janssens-Maenhout, G. (2018). Gridded emissions of air pollutants for the period
884 1970–2012 within EDGAR v4. 3.2. *Earth Syst. Sci. Data*, 10(4), 1987-2013.
- 885 Da Silva, V. D. P. R., e Silva, R. A., Cavalcanti, E. P., Braga, C. C., de Azevedo, P. V.,
886 Singh, V. P., & Pereira, E. R. R. (2010). Trends in solar radiation in NCEP/NCAR
887 database and measurements in northeastern Brazil. *Solar Energy*, 84(10), 1852-
888 1862.
- 889 de Jong, P., Barreto, T. B., Tanajura, C. A., Kouloukoui, D., Oliveira-Esquerre, K. P.,
890 Kiperstok, A., & Torres, E. A. (2019). Estimating the impact of climate change on
891 wind and solar energy in Brazil using a South American regional climate model.
892 *Renewable energy*, 141, 390-401.
- 893 de Lima, F. J. L., Martins, F. R., Costa, R. S., Gonçalves, A. R., dos Santos, A. P. P., &
894 Pereira, E. B. (2019). The seasonal variability and trends for the surface solar
895 irradiation in northeastern region of Brazil. *Sustainable Energy Technologies and*
896 *Assessments*, 35, 335-346.
- 897 Doelling, D. R., Loeb, N. G., Keyes, D. F., Nordeen, M. L., Morstad, D., Nguyen, C., ... &
898 Sun, M. (2013). Geostationary enhanced temporal interpolation for CERES flux
899 products. *Journal of Atmospheric and Oceanic Technology*, 30(6), 1072-1090.
- 900 Doelling, D. R., Sun, M., Nordeen, M. L., Haney, C. O., Keyes, D. F., & Mlynchak, P. E.
901 (2016). Advances in geostationary-derived longwave fluxes for the CERES synoptic
902 (SYN1deg) product. *Journal of Atmospheric and Oceanic Technology*, 33(3), 503-
903 521.
- 904 Driemel, A., Augustine, J., Behrens, K., Colle, S., Cox, C., Cuevas-Agulló, E., ... & König-
905 Langlo, G. (2018). Baseline Surface Radiation Network (BSRN): structure and data
906 description (1992–2017). *Earth System Science Data*, 10(3), 1491-1501.
- 907 Dutton, E. G., Stone, R. S., Nelson, D. W., & Mendonca, B. G. (1991). Recent interannual
908 variations in solar radiation, cloudiness, and surface temperature at the South Pole.
909 *Journal of Climate*, 4(8), 848-858.

- 910 Feng, F., & Wang, K. (2019). Determining factors of monthly to decadal variability in
911 surface solar radiation in China: Evidences from current reanalyses. *Journal of*
912 *Geophysical Research: Atmospheres*, 124(16), 9161-9182.
- 913 Ferreira, G. W., & Reboita, M. S. (2022). A new look into the South America precipitation
914 regimes: Observation and Forecast. *Atmosphere*, 13(6), 873.
- 915 Fisch, G., MARENGO, J. A., & NOBRE, C. A. (1998). Uma revisão geral sobre o clima da
916 Amazônia. *Acta amazônica*, 28, 101-101.
- 917 Gilgen, H., Roesch, A., Wild, M., & Ohmura, A. (2009). Decadal changes in shortwave
918 irradiance at the surface in the period from 1960 to 2000 estimated from Global
919 Energy Balance Archive Data. *Journal of Geophysical research: atmospheres*,
920 114(D10).
- 921 Gueymard, C. A., & Yang, D. (2020). Worldwide validation of CAMS and MERRA-2
922 reanalysis aerosol optical depth products using 15 years of AERONET
923 observations. *Atmospheric Environment*, 225, 117216.
- 924 Hakuba, M. Z., Folini, D., & Wild, M. (2016). On the zonal near-constancy of fractional solar
925 absorption in the atmosphere. *Journal of Climate*, 29(9), 3423-3440.
- 926 Hersbach, H., Bell, B., Berrisford, P., Hirahara, S., Horányi, A., Muñoz-Sabater, J., ... &
927 Thépaut, J. N. (2020). The ERA5 global reanalysis. *Quarterly Journal of the Royal*
928 *Meteorological Society*, 146(730), 1999-2049.
- 929 IBGE. Censo Demográfico. Rio de Janeiro, Brazil: Fundação Instituto Brasileiro de
930 Geografia e Estatística. 2022. Available at:
931 <https://censo2022.ibge.gov.br/panorama/index.html> Last access: 01 Nov. 2023.
932 <https://censo2022.ibge.gov.br/panorama/index.html>
- 933 Inness, A., Ades, M., Agustí-Panareda, A., Barré, J., Benedictow, A., Blechschmidt, A. M., ...
934 & Suttie, M. (2019). The CAMS reanalysis of atmospheric composition.
935 *Atmospheric Chemistry and Physics*, 19(6), 3515-3556.
- 936 Jiao, B., Su, Y., Li, Q., Manara, V., & Wild, M. (2023). An integrated and homogenized
937 global surface solar radiation dataset and its reconstruction based on a convolutional
938 neural network approach. *Earth System Science Data*.
- 939 Kambezidis, H. D., Kaskaoutis, D. G., Kharol, S. K., Moorthy, K. K., Satheesh, S. K.,
940 Kalapureddy, M. C. R., ... & Wild, M. (2012). Multi-decadal variation of the net
941 downward shortwave radiation over south Asia: The solar dimming effect.
942 *Atmospheric Environment*, 50, 360-372.
- 943 Kendall, M. G. (1975). Rank correlation methods. 2nd impression. *Charles Griffin and*
944 *Company Ltd. London and High Wycombe*.
- 945 Kudo, R., Uchiyama, A., Ijima, O., Ohkawara, N., & Ohta, S. (2012). Aerosol impact on the
946 brightening in Japan. *Journal of Geophysical Research: Atmospheres*, 117(D7).
- 947 Li, Z., Barker, H. W., & Moreau, L. (1995). The variable effect of clouds on atmospheric
948 absorption of solar radiation. *Nature*, 376(6540), 486-490.
- 949 Liepert, B. G. (2002). Observed reductions of surface solar radiation at sites in the United
950 States and worldwide from 1961 to 1990. *Geophysical research letters*, 29(10), 61-1.
- 951 Liley, J. B. (2009). New Zealand dimming and brightening. *Journal of Geophysical*
952 *Research: Atmospheres*, 114(D10).

- 953 Lobo, C., & Cunha, J. M. P. D. (2019). Migração e mobilidade pendular nas áreas de
954 influência de metrópoles brasileiras. *Mercator (Fortaleza)*, 18.
- 955 Loeb, N. G., Doelling, D. R., Wang, H., Su, W., Nguyen, C., Corbett, J. G., ... & Kato, S.
956 (2018). Clouds and the earth's radiant energy system (CERES) energy balanced and
957 filled (EBAF) top-of-atmosphere (TOA) edition 4.0 data product. *Journal of*
958 *Climate*, 31(2), 895-918.
- 959 Long, C. N., & Dutton, E. G. (2002). BSRN Global Network Recommended QC Tests, V2.
960 0, BSRN Technical Report.
- 961 Long, C. N., Dutton, E. G., Augustine, J. A., Wiscombe, W., Wild, M., McFarlane, S. A., &
962 Flynn, C. J. (2009). Significant decadal brightening of downwelling shortwave in the
963 continental United States. *Journal of Geophysical Research: Atmospheres*,
964 114(D10).
- 965 Madhavan, B. L., Deneke, H., Witthuhn, J., & Macke, A. (2017). Multiresolution analysis of
966 the spatiotemporal variability in global radiation observed by a dense network of 99
967 pyranometers. *Atmospheric Chemistry and Physics*, 17(5), 3317-3338.
- 968 Manara, V., Brunetti, M., Celozzi, A., Maugeri, M., Sanchez-Lorenzo, A., & Wild, M.
969 (2016). Detection of dimming/brightening in Italy from homogenized all-sky and
970 clear-sky surface solar radiation records and underlying causes (1959–2013).
971 *Atmospheric Chemistry and Physics*, 16(17), 11145-11161.
- 972 Mann, H. B. (1945). Nonparametric tests against trend. *Econometrica: Journal of the*
973 *econometric society*, 245-259.
- 974 Nishizawa, S., & Yoden, S. (2005). Distribution functions of a spurious trend in a finite
975 length data set with natural variability: Statistical considerations and a numerical
976 experiment with a global circulation model. *Journal of Geophysical Research:*
977 *Atmospheres*, 110(D12).
- 978 Norris, J. R., & Wild, M. (2007). Trends in aerosol radiative effects over Europe inferred
979 from observed cloud cover, solar “dimming,” and solar “brightening”. *Journal of*
980 *Geophysical Research: Atmospheres*, 112(D8).
- 981 Ohmura, A., & Lang, H. (1989). Secular variation of global radiation over Europe, in *Current*
982 *Problems in Atmospheric Radiation*. edited by J. Lenoble, & JF Geleyn, 98, 301.
- 983 Ohmura, A., Dutton, E. G., Forgan, B., Fröhlich, C., Gilgen, H., Hegner, H., ... & Wild, M.
984 (1998). Baseline Surface Radiation Network (BSRN/WCRP): New precision
985 radiometry for climate research. *Bulletin of the American Meteorological Society*,
986 79(10), 2115-2136.
- 987 Ohmura, A. (2009). Observed decadal variations in surface solar radiation and their causes.
988 *Journal of Geophysical Research: Atmospheres*, 114(D10).
- 989 Pfeifroth, U., Sanchez-Lorenzo, A., Manara, V., Trentmann, J., & Hollmann, R. (2018).
990 Trends and variability of surface solar radiation in Europe based on surface-and
991 satellite-based data records. *Journal of Geophysical Research: Atmospheres*,
992 123(3), 1735-1754.
- 993 Power, H. C. (2003). Trends in solar radiation over Germany and an assessment of the role of
994 aerosols and sunshine duration. *Theoretical and Applied Climatology*, 76(1), 47-63.
- 995 Raichijk, C. (2012). Observed trends in sunshine duration over South America. *International*
996 *Journal of Climatology*, 32(5), 669-680.

- 997 Reboita, M. S., Gan, M. A., Da Rocha, R. P., & Ambrizzi, T. (2010). Precipitation regimes in
998 South America: a bibliography review. *Revista Brasileira de Meteorologia*, 25(2),
999 185-204.
- 1000 Rosário, N. E., Sauini, T., Pauliquevis, T., Barbosa, H. M., Yamasoe, M. A., & Barja, B.
1001 (2019). Aerosol optical depth retrievals in central Amazonia from a multi-filter
1002 rotating shadow-band radiometer calibrated on-site. *Atmospheric Measurement*
1003 *Techniques*, 12(2), 921-934.
- 1004 Russak, V. (1990). Trends of solar radiation, cloudiness and atmospheric transparency during
1005 recent decades in Estonia. *Tellus B*, 42(2), 206-210.
- 1006 Schwartz, R. D. (2005). Global dimming: Clear-sky atmospheric transmission from
1007 astronomical extinction measurements. *Journal of Geophysical Research:*
1008 *Atmospheres*, 110(D14).
- 1009 Schwarz, M., Folini, D., Hakuba, M. Z., & Wild, M. (2018). From point to area: Worldwide
1010 assessment of the representativeness of monthly surface solar radiation records.
1011 *Journal of Geophysical Research: Atmospheres*, 123(24), 13-857.
- 1012 Schwarz, M., Folini, D., Yang, S., & Wild, M. (2019). The annual cycle of fractional
1013 atmospheric shortwave absorption in observations and models: spatial structure,
1014 magnitude, and timing. *Journal of Climate*, 32(20), 6729-6748.
- 1015 Sen, P. K. (1968). Estimates of the regression coefficient based on Kendall's tau. *Journal of*
1016 *the American statistical association*, 63(324), 1379-1389.
- 1017 Silva Junior, C. H., Pessôa, A. C., Carvalho, N. S., Reis, J. B., Anderson, L. O., & Aragão, L.
1018 E. (2021). The Brazilian Amazon deforestation rate in 2020 is the greatest of the
1019 decade. *Nature ecology & evolution*, 5(2), 144-145.
- 1020 Stjern, C. W., Kristjánsson, J. E., & Hansen, A. W. (2009). Global dimming and global
1021 brightening—An analysis of surface radiation and cloud cover data in northern
1022 Europe. *International Journal of Climatology: A Journal of the Royal*
1023 *Meteorological Society*, 29(5), 643-653.
- 1024 Torres, O., Tanskanen, A., Veihelmann, B., Ahn, C., Braak, R., Bhartia, P. K., ... & Levelt, P.
1025 (2007). Aerosols and surface UV products from Ozone Monitoring Instrument
1026 observations: An overview. *Journal of Geophysical Research: Atmospheres*,
1027 112(D24).
- 1028 Vera, C., Baez, J., Douglas, M., Emmanuel, C. B., Marengo, J., Meitin, J., ... & Zipser, E.
1029 (2006). The South American low-level jet experiment. *Bulletin of the American*
1030 *Meteorological Society*, 87(1), 63-78.
- 1031 Wang, C., Jeong, G. R., & Mahowald, N. (2009). Particulate absorption of solar radiation:
1032 anthropogenic aerosols vs. dust. *Atmospheric Chemistry and Physics*, 9(12), 3935-
1033 3945.
- 1034 Wang, K., Ma, Q., Li, Z., & Wang, J. (2015). Decadal variability of surface incident solar
1035 radiation over China: Observations, satellite retrievals, and reanalyses. *Journal of*
1036 *Geophysical Research: Atmospheres*, 120(13), 6500-6514.
- 1037 Wang, X. L. (2008). Penalized maximal F test for detecting undocumented mean shift
1038 without trend change. *Journal of Atmospheric and Oceanic Technology*, 25(3), 368-
1039 384.

- 1040 Wild, M. (2009). Global dimming and brightening: A review. *Journal of Geophysical*
1041 *Research: Atmospheres*, 114(D10).
- 1042 Wild, M., Wacker, S., Yang, S., & Sanchez-Lorenzo, A. (2021). Evidence for clear-sky
1043 dimming and brightening in central Europe. *Geophysical Research Letters*, 48(6),
1044 e2020GL092216.
- 1045 Yamasoe, M. A., Rosário, N. M. É., Almeida, S. N. S. M., & Wild, M. (2021). Fifty-six years
1046 of surface solar radiation and sunshine duration over São Paulo, Brazil: 1961–2016.
1047 *Atmospheric Chemistry and Physics*, 21(9), 6593-6603.
- 1048 Yang, S., Wang, X. L., & Wild, M. (2018). Homogenization and trend analysis of the 1958–
1049 2016 in situ surface solar radiation records in China. *Journal of Climate*, 31(11),
1050 4529-4541.
- 1051 Yuan, M., Leirvik, T., & Wild, M. (2021). Global trends in downward surface solar radiation
1052 from spatial interpolated ground observations during 1961–2019. *Journal of*
1053 *Climate*, 34(23), 9501-9521.
- 1054 Zuluaga, C. F., Avila-Diaz, A., Justino, F. B., & Wilson, A. B. (2021). Climatology and
1055 trends of downward shortwave radiation over Brazil. *Atmospheric Research*, 250,
1056 105347.

1057 Appendix

Station	Composite	Coordinates	Does it include SYNOP cloud cover?	% of monthly data available
Manaus	Manaus region	3.10S 60.01W	yes	87
Coari	Manaus region	4.10S 63.14W	yes	74
Rio Urubu	Manaus region	2.63S 59.60W	no	75
Urucará	Manaus region	2.53S 57.75W	no	82
Belém	Belém region	1.41S 48.43W	yes	95
Castanhal	Belém region	1.30S 47.94W	no	71
Tucuruí	Belém region	3.82S 49.67W	yes	92
Salinópolis	Belém region	0.62S 47.35W	no	69
Alta Floresta	South Amazon	10.07S 56.17W	no	62
Ariquemes	South Amazon	9.94S 62.96W	no	73
Juína	South Amazon	11.37S 58.77W	no	78
Porto Velho	South Amazon	8.79S 63.84W	no	73
Sorriso	South Amazon	12.55S 55.72W	no	85
Fortaleza	Fortaleza region	3.81S 38.53W	yes	68
Areia	Fortaleza region	6.97S 35.71W	yes	85

Caicó	Fortaleza region	6.46S 37.08W	yes	68
Natal	Fortaleza region	5.83S 35.20W	yes	65
Brasília	Midwest	15.78S 47.92W	yes	84
Goiânia	Midwest	16.64S 49.22W	yes	94
Campo Grande	Midwest	20.44S 54.72W	yes	79
Salvador	Salvador region	13.00S 38.50W	yes	89
Cruz das Almas	Salvador region	12.67S 39.08W	yes	66
Feira de Santana	Salvador region	12.19S 38.96W	yes	64
Itirucu	Salvador region	13.52S 40.11W	yes	61
Curitiba	South	25.44S 49.23W	yes	72
Porto Alegre	South	30.05S 51.17W	yes	95
Santa Maria	South	29.72S 53.72W	yes	89
Florianópolis*	South	27.60S 48.52W	yes	
Campos do Jordão	Southeast	22.75S 45.60W	yes	69
Monte Verde	Southeast	22.86S 46.04W	no	84
Rio de Janeiro - Marambaia	Southeast	23.05S 43.59W	yes	78
Seropédica	Southeast	22.75S 43.68W	no	98
São Paulo*	Southeast	23.65S 46.62W	yes	99

1058

1059

1060

1061

1062

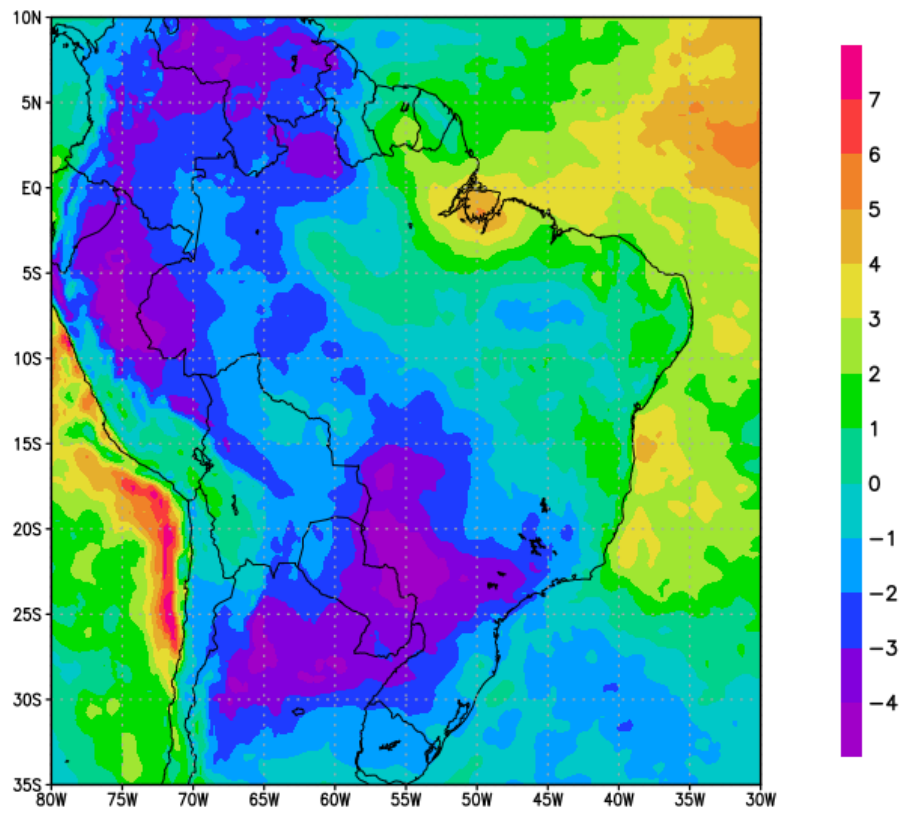
1063

1064

1065

1066

Table 32: Stations used in the study, the composites they were associated with, their coordinates, and information whether Synop cloud cover data was available and the percentage of months with available data (out of all the months in the period used for the respective composite - see table 1). *Stations not from the Brazilian National Institute of Meteorology. Florianópolis station from BSRN; São Paulo station from the Institute for Astronomy, Geophysics and Atmospheric Sciences at the University of São Paulo.



1067

1068 **Figure A1 - Total cloud cover trends for the 1990-2006 period (in % per decade) from ERA5.**